JGR Atmospheres

RESEARCH ARTICLE
10.1029/2021JD035540

The Balance Between Heterogeneous and Homogeneous Nucleation of Ice Clouds Using CAM5/CARMA

Christopher Maloney[1,2], Brian Toon[1,2], Charles Bardeen[3], Pengfei Yu[4], Karl Froyd[5,6], Jennifer Kay[1], and Sarah Woods[7]

[1]University of Colorado Boulder, Boulder, CO, USA, [2]Laboratory for Atmospheric and Space Physics, Boulder, CO, USA, [3]National Center for Atmospheric Research, Boulder, CO, USA, [4]Jinan University, Guangzhou, China, [5]National Oceanic and Atmospheric Administration, Boulder, CO, USA, [6]Cooperative Institute for Research in Environmental Sciences, Boulder, CO, USA, [7]Spec Inc, Boulder, CO, USA

Key Points:

- Interactive aerosols and heterogeneous nucleation are added to the CAM5/CARMA sectional ice model
- Simulated dust profiles compare better to Particle Analysis by Laser Mass Spectrometry observations as a result of our CAM5/CARMA modifications
- Mixed phase clouds in the mid-latitudes are the most impacted by the addition of heterogeneous nucleation in Community Aerosol and Radiation model for Atmospheres (CARMA)

Correspondence to:

C. Maloney,
christopher.maloney@colorado.edu

Citation:

Maloney, C., Toon, B., Bardeen, C., Yu, P., Froyd, K., Kay, J., & Woods, S. (2022). The balance between heterogeneous and homogeneous nucleation of ice clouds using CAM5/CARMA. *Journal of Geophysical Research: Atmospheres*, *127*, e2021JD035540. https://doi.org/10.1029/2021JD035540

Received 9 JUL 2021
Accepted 9 FEB 2022

Author Contributions:

Conceptualization: Christopher Maloney, Brian Toon, Charles Bardeen
Data curation: Christopher Maloney, Karl Froyd, Sarah Woods
Formal analysis: Christopher Maloney
Funding acquisition: Brian Toon
Investigation: Christopher Maloney
Methodology: Christopher Maloney, Brian Toon, Charles Bardeen, Pengfei Yu
Project Administration: Brian Toon
Resources: Brian Toon, Karl Froyd
Software: Charles Bardeen, Pengfei Yu
Supervision: Brian Toon
Validation: Christopher Maloney, Brian Toon, Charles Bardeen, Jennifer Kay
Visualization: Christopher Maloney, Charles Bardeen
Writing – original draft: Christopher Maloney
Writing – review & editing: Brian Toon, Charles Bardeen, Pengfei Yu, Karl Froyd, Jennifer Kay, Sarah Woods

Abstract We present a modification to the Community Aerosol and Radiation model for Atmospheres (CARMA) sectional ice microphysical model where we have added interactive nucleation of sulfates and heterogeneous nucleation onto dust in order to create a more comprehensive representation of ice nucleation within the CARMA sectional ice model. The Yu et al. (2019, https://doi.org/10.1029/2018gl080544) convective wet removal fix has also been added in order to correctly transport aerosol within the Community Atmosphere Model version 5 (CAM5) and the 3-mode Modal Aerosols Model (MAM3). In CARMA, the balance of homogeneous and heterogeneous nucleation is controlled by the presence of temperatures below 240 K, supersaturation, and the availability of heterogeneous nuclei. Due to a paucity of dust at altitudes above about 7 km, where temperatures over most of the Earth fall below 240 K, cirrus clouds above 7 km nucleate primarily via homogeneous nucleation on aqueous sulfate aerosols in our simulations. Over mid-latitudes of the Northern Hemisphere, dust is more common above 7 km during spring through fall, and both heterogeneous nucleation and homogenous freezing occur in our model. Below 7 km heterogeneous nucleation dominates in situ formation of ice. Furthermore, we find an improvement of the representation of in-cloud ice within mixed phase clouds in CAM5/CARMA when compared to simulations with only homogeneous ice nucleation. Other modes of nucleation such as contact nucleation of liquid cloud droplets or liquid cloud droplet freezing on immersion nuclei, were not directly compared with classical depositional heterogeneous nucleation in this study.

Plain Language Summary The work presented here modified ice nucleation within the Community Aerosol and Radiation model for Atmospheres cirrus model in two ways. The first modification introduced an evolving sulfate aerosol field in place of the current sulfate climatology, while the second modification added depositional heterogeneous nucleation of ice onto dust. This work also adapted a fix to the wet removal of aerosols within convection from a previous study. This fix leads to a better representation of the vertical transport of aerosols within version 5 of the Community Atmosphere Model (CAM5). Simulations show that the addition of heterogeneous nucleation improves dust mass when compared to aircraft observations. Over the mid-latitudes in the Northern Hemisphere, dust is commonly found above 7 km in altitude and both heterogeneous and homogeneous nucleation occurs over the course of the year. Simulated cirrus ice clouds experience only minor impacts from the added nucleation schemes presented in this work, but our results show that the addition of heterogeneous nucleation improves the representation of in-cloud ice, especially within mixed phase clouds when compared to simulations without heterogeneous nucleation.

1. Introduction

Ice clouds cover approximately 20%–25% of Earth's surface at any given time (Rossow & Schiffer, 1999; P.-H. Wang et al., 1994). As a result, cirrus play a significant role in climate. For example, ice clouds substantially influence Earth's radiation budget (Comstock et al., 2002; Yang et al., 2010). Cirrus are also known to dehydrate air as it enters the stratosphere (e.g., Jensen et al., 1996, 2010, 2017) and can potentially influence the tropical troposphere-stratosphere exchange through thermal lifting (Corti et al., 2006; Jensen et al., 2011).

The in situ formation of ice crystals in cirrus can follow two pathways. At low temperatures and high supersaturations, ice crystals form spontaneously (homogeneous nucleation) from aqueous aerosols mostly comprised of solutions of sulfates, but possibly also nitrates, organics, or sea salt. Homogeneously formed cirrus clouds

are characterized by high concentrations of small ice crystals which rapidly deplete the surrounding air of water vapor (e.g., Jensen & Pfister, 2004; Jensen et al., 1998, 2010). Studies have shown that the onset of homogeneous nucleation depends on the water activity of the aerosols (Koop et al., 2000), rather than the solute composition.

Ice can also form via the freezing of water vapor onto insoluble ice nucleating particles (INP) or the immersion of INP in supercooled water. This freezing pathway, also known as heterogeneous nucleation, occurs at warmer temperatures and lower supersaturations than homogeneous nucleation. Heterogeneously formed cirrus clouds possess fewer, larger ice crystals compared to their homogeneously formed counterparts since insoluble ice nuclei generally are much less abundant than aqueous aerosols. However, when enough INP are present heterogeneous nucleation can lower the ambient saturation enough to delay or even prevent the onset of homogeneous nucleation (Liu, Easter, et al., 2012).

While we have a general understanding of cirrus formation processes, there are still considerable gaps in our knowledge. For example, within the tropical tropopause layer (TTL), which can be found just above the level of convective outflow (∼14 km) and below 18.5 km (Fueglistaler et al., 2009), limited in situ observations have made it difficult to verify the mechanisms of ice formation. In the TTL, sedimentation associated with cirrus clouds dehydrates air as it ascends to the stratosphere (Jensen et al., 1996; Randel & Jensen, 2013; Rosenfield et al., 1998). However, individual cirrus clouds can possess ice formed via different nucleation mechanisms, which can make predicting the properties of ice clouds difficult. For example, Jensen, Diskin, et al. (2013) noted thin embedded layers of high ice concentrations between low ice concentration layers within a single cirrus cloud. They concluded that the high concentration layers were likely homogeneously formed from wave activity. However, they could not answer why low ice concentration layers occurred when the entire cloud experienced conditions conducive to homogeneous nucleation.

The ambiguity associated with ice formation in cirrus contributes to the overall uncertainty in simulations of clouds and cloud-radiation feedbacks within general circulation models (GCM's, e.g., Rasch & Kristjánsson, 1998; Ringer et al., 2006; Waliser et al., 2009, Zhang et al., 2005). Regardless, numerous studies have been undertaken to advance ice cloud representation within GCM's. For example, Kärcher and Burkhardt (2008) showed that a process-oriented approach for the representation of ice supersaturation, microphysics, and the grid-box fractional coverage of cirrus clouds from statistical distributions can produce more realistic ice clouds than traditional GCM cloud schemes which use relative humidity based cloud fraction schemes. More recently the Community Aerosol and Radiation model for Atmospheres microphysical model (CARMA, Toon et al., 1988; Turco et al., 1979) was coupled with the widely used Community Earth System Model's (CESM1) atmospheric component (CAM5) in an effort to improve ice cloud representation within CAM5 (Bardeen et al., 2013). Coupling CARMA with CAM5 (CAM5/CARMA from here on) has been shown to improve the global representation of cirrus clouds (Bardeen et al., 2013), as well as TTL cirrus (Maloney et al., 2019) within CESM1.

The work presented here provides an intermediate modification to the CAM5/CARMA model which focuses on improving the treatment of ice nucleation. The current implementation of the CARMA cirrus model only performs homogeneous nucleation of in situ ice with sulfate aerosols provided by a climatology from a previous study by English et al. (2011). In the study presented here, we replace the static climatology with a set of interactive sulfate aerosols provided by the 3 mode, Modal Aerosol Model (MAM3, Liu, Shi, et al., 2012). A basic heterogeneous nucleation scheme performing depositional nucleation of ice onto dust has also been included in an effort to evaluate CARMA's representation of ice when heterogeneous nucleation is also included. Lastly, this study has implemented the Yu et al. (2019) fix to the wet removal of aerosols within convection, that improves the simulation of dust concentrations in the upper troposphere.

It should be noted that only ice nucleation and cloud formation is being addressed in CAM5/CARMA in this study. Furthermore, ice can form via in situ freezing or as detrainment from convection within CARMA. We purely focus on the in situ formation of ice in this study. The updated in situ ice cloud formation in CARMA is evaluated by a suite of satellite and aircraft observations, each of which is described in Section 2 of this article. The results of this study can be found in Section 3, while Section 4 provides a brief discussion of these findings. A summary and suggested future work can be found in Section 5.

2. Model Overview

2.1. The Community Aerosols and Radiation Model for Atmospheres

CARMA is a sectional cloud and aerosol model that treats the particle size distribution using a set of mass bins. CARMA is flexible so that the number of bins can be varied and multiple constituents can be tracked within the bins. Consequently, there are CARMA models for a wide variety of aerosols and clouds. This study uses the CARMA-cirrus model (Bardeen et al., 2008, 2013) with recent modifications to TTL cloud representation from Maloney et al. (2019) included. The CARMA-cirrus model replaces the Morrison and Gettelman (2008) two-moment ice microphysics from CAM5 (Bardeen et al., 2013). As a sectional model, CARMA-cirrus employs a size distribution with 28 uniquely sized bins. Ice is repartitioned into two types in CARMA-cirrus: (a) in situ ice formed via homogeneous nucleation of sulfate aerosols or heterogeneous nucleation on dust aerosols (referred to as in situ ice from here on) and (b) convectively detrained ice provided by the bulk convective parameterizations in CAM5 (referred to as detrained ice from here on). Detrained ice is defined as the ice crystals left behind by the lateral spreading of convective cores. Detrained ice is treated as a separate group of particles from in situ ice. CARMA ice bins start at a radius of ∼0.5 μm and have a max size of ∼300 μm for in situ ice and 1,000 μm for detrained ice. These bins contain information about the mass of in situ ice, the mass of detrained ice, and the mass of sulfate or dust on which in situ ice forms. For detrained ice, density of the ice changes with each bin in order to capture changes in shape, such as in the case of ice becoming snow (Bardeen et al., 2013).

The two-moment Morrison and Gettelman (2008) model within CAM5 still handles all of the liquid microphysics except for the Bergeron-Findeisen process, the melting of ice, and the freezing of liquid drops. Each of these processes are handled by CARMA, which converts the gamma size distribution assumed by the two-moment microphysics (Morrison & Gettelman, 2008) into sectional bins for CARMA processing (Bardeen et al., 2013). At the end of each simulation time step the binned distributions are converted back into the two-moment form for the CAM5 physics.

The bulk convective parameterization from CAM5 provides CARMA with detrained ice mass. Once passed to CARMA, the cirrus model applies the spherical mass-diameter relationship introduced in Heymsfield et al. (2010) to relate the detrained ice mass to particle size, which is then used to populate the detrained ice bins. Temperature is then used to determine the phase of detrained condensate. All detrained condensate is considered to be ice at temperatures less than −20°C while all condensate is considered to be liquid at temperatures warmer than 0°C. Between −20°C and 0°C a linear ramp is used to determine the phase of water.

Ice cloud fraction and the sub-grid supersaturation in CARMA follows a modified Wilson and Ballard (1999) scheme, which determines the sub-grid cloud fraction and supersaturation based upon a tunable, critical relative humidity and mixing ratio. For a more in-depth discussion about how ice cloud fraction and sub-grid supersaturation are handled within CARMA, we direct the reader to Bardeen et al. (2013) and Maloney et al. (2019).

2.2. The Modal Aerosol Model

Aerosol is handled by the 3-mode, Modal Aerosol Model (MAM3) described by Liu, Shi, et al. (2012) in CESM1. The three modes within MAM3 are the Aitken (0.015–0.053 μm), accumulation (0.058–0.27 μm), and coarse (0.8–3.65 μm) aerosol modes. MAM3 assumes lognormal distributions for each aerosol mode with a prescribed geometric standard deviation (Easter et al., 2004). A total of 15 aerosol species are tracked by MAM3 (Liu, Shi, et al., 2012), so each mode contains multiple chemical species. Of relevance to the current article are dust and sulfate.

2.3. Interactive Sulfates in CARMA

In this study, we use an aerosol population provided by MAM3 which responds to the removal or addition of aerosols when ice nucleates or sublimates. MAM3 tracks the mass mixing ratio for each aerosol species within a mode. Number mixing ratio is represented by a single, combined value for all aerosol species within a mode. MAM3 assumes that aerosol modes are internally mixed within modes and external mixed among modes (Liu, Shi, et al., 2012). However, for the purposes of droplet activation and nucleation onto aerosols, CAM5 assumes external mixtures in order to save computational time. We also make this assumption in our heterogeneous

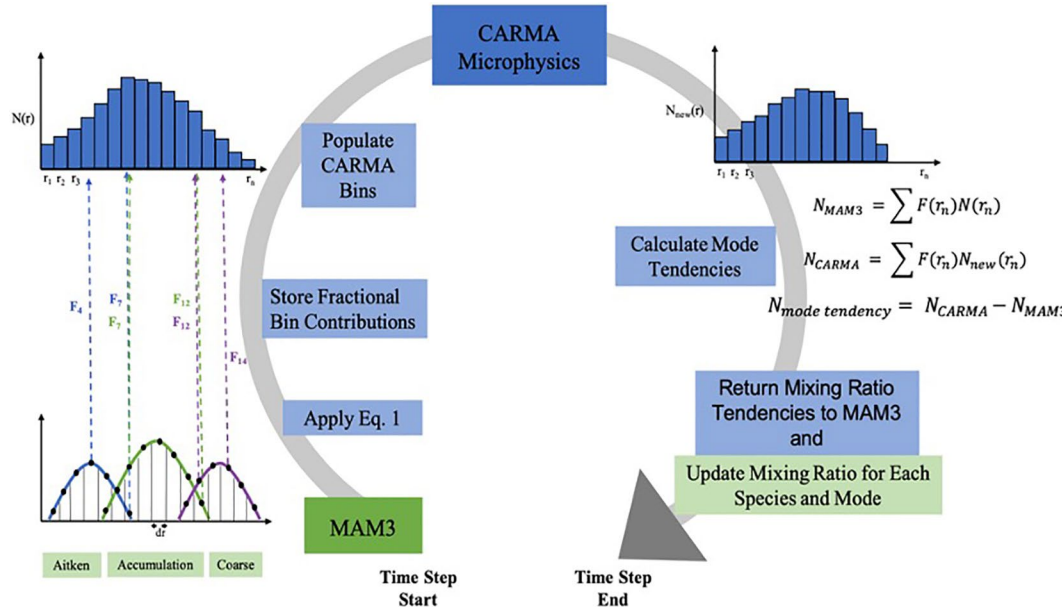

Figure 1. A diagram of the transfer of information between MAM3 and CARMA for interactive aerosols. Green shading indicates an MAM3 processe, while blue shading indicates a CARMA process. $N[r]$ represents the mixing ratio brought in from MAM3 pre-CARMA microphysics, while $N_{new}[r]$ represents the mixing ratio post CARMA microphysics. $F[r_n]$ is the fractional contribution from each MAM3 mode to each CARMA bin.

nucleation implementation for ice. In order to be used within CARMA, the lognormal distribution of each mode's number concentration is mapped onto a binned size distribution using Equation 1

$$N(r) = \frac{N * dr}{\sqrt{2\pi} * r * \ln \sigma_g} \exp\left[-\left(\frac{(\ln r - \ln r_m)^2}{2 \ln^2 \sigma_g}\right)\right] \quad (1)$$

where N is the total aerosol concentration for the mode while r and dr represent the mean bin radius and the bin width respectively. r_m represents the dry mean particle radius of the mode, and σ_g represents the distribution variance.

This mapping is done in order to allow for the modal aerosols to interact with the bin microphysics. CARMA retains information about the aerosols in ice (cloud-borne aerosols), but the interstitial aerosol state is maintained by MAM and thus requires an update to the interstitial aerosol tendencies at the end of every time step after CARMA has performed nucleation. Figure 1 shows a flowchart of this mapping process. First, mixing ratios from MAM3 are read into CARMA where Equation 1 is applied to map the modal values into bins centered around a radius "r" with width "dr" (black dots, bottom left, Figure 1). Where modes overlap, a sum of the contribution from each mode is calculated in order to obtain the total mixing ratio in each bin (colored arrows, middle left, Figure 1). During the summation process, the fractional contribution to the binned mixing ratio from each MAM3 mode (e.g., F_7 or F_{12}, in Figure 1) is calculated and stored to later calculate aerosol tendencies. The "total" binned distribution ($N(r)$, upper left, Figure 1) then serves as the ambient aerosol population for CARMA to use in the ice microphysics. After the CARMA microphysics concludes, the modified binned distribution ($N_{new}(r)$, upper right, Figure 1) is summed across all bins to obtain a single mixing ratio value for each mode (middle right, Figure 1). In order to identify the changes to mass and number in each mode, the previously calculated fractional contribution of each mode to each bin is applied during this summation. This application of $F(r_n)$ ensures that mass is conserved and prevents CARMA from erroneously changing the aerosol mixing ratio when no ice nucleation occurs. At the end of each model time step a mixing ratio tendency is computed by taking the difference of the summed CARMA mixing ratios (N_{CARMA}, Figure 1) and the initial MAM3 mixing ratios (N_{MAM3}, Figure 1). The resulting tendency values are then given to MAM3 to be used to update the overall aerosol populations. The net result of this parameterization is an ever-evolving aerosol field that is sensitive to ice nucleation.

It is important to note that the number mixing ratio requires the extra step of separating out the contribution to the mode number mixing ratio from each aerosol species. Mass is used to determine an individual species contribution to the mode's total mass mixing ratio. This fractional contribution is then applied to the mode number mixing ratio to determine how much of the mode number mixing ratio is made up of a particular aerosol species. For example, if dust contributes to 25% of the total mass mixing ratio, then it will be assumed that dust also comprises 25% of the total number.

2.4. Ice Nucleation in CARMA

By default, in situ ice in CARMA is formed via the homogeneous freezing of aqueous sulfate aerosols based upon the Koop et al. (2000) scheme, which determines nucleation rates based upon temperature and water activity. It is notable that temperatures must be colder than 240 K for homogeneous nucleation to occur.

Due to our modifications, in situ heterogeneous nucleation of ice is now conducted in CARMA. Observations of aerosols within ice crystals in the TTL suggest that nucleation is dominated by sulfate and organic particles, although ice concentrations were much lower than would be expected by homogeneous nucleation (Froyd et al., 2010). However, similar data from lower altitude cirrus and mixed phase clouds show that INP, especially dust, dominate the nucleation process (Cziczo et al., 2013). It is possible that the nucleation properties of different compositions of dust might vary. However, Demott et al. (2010) suggested that our knowledge of the parameters used in theories of ice nucleation was too limited to explore how changes in populations of INP might affect simulated clouds. Numerous studies have made a compelling case that when INP are present, heterogeneous nucleation can play a significant role in UT/LS ice nucleation (e.g., Froyd et al., 2010; Jensen et al., 2018; Jensen, Lawson, et al., 2013; Lohmann, 2002). With this context in mind, we added a basic heterogeneous nucleation scheme to CARMA as a first step in enabling the model to capture this important missing microphysical feature.

The heterogeneous nucleation scheme added to CARMA applies classical nucleation theory following Keese (1989), Pruppacher and Klett (1997), and Rapp and Thomas (2006). In order for heterogeneous nucleation to occur, temperature must drop below the triple point of water (273.16 K) and sufficient supersaturation with respect to ice must occur. INP concentration and wettability (i.e., contact parameter) also impact the onset of heterogeneous nucleation. INP size plays an important role in determining the nucleation rates. Ice will nucleate onto dust in the larger-sized CARMA bins first. We also note that a lower aerosol concentration limit of 1×10^{-6} cm^{-3} is used to bypass ice microphysics within CARMA when few particles are present. Only water vapor deposition onto INP is performed by this heterogeneous nucleation scheme. Other potential heterogeneous nucleation methods such as immersion freezing of liquid water droplets, or of aerosols, are not included.

It was previously mentioned that supersaturation within CARMA follows a modified version of the Wilson and Ballard (1999) scheme. Within this scheme, sub-grid supersaturation with respect to ice (S_{ice}) is represented by:

$$S_{\text{ice}} = \frac{q_v - \alpha q_{\text{sat,ice}}}{q_{\text{sat,ice}}} \tag{2}$$

where q_v is the water vapor mixing ratio, $q_{\text{sat,ice}}$ is the ice saturation mixing ratio, and α is represented by Equation 3.

$$\alpha = \text{RH}_{\text{crit}}(1 - cf) + cf \tag{3}$$

RH_{crit} in Equation 3 represents the grid box critical relative humidity needed for ice cloud formation and cf is the grid box cloud fraction. RH_{crit} equals 0.7 for the simulations performed in this study, but RH_{crit} is a tunable parameter (Bardeen et al., 2013).

Mineral dust was chosen for heterogeneous nucleation because dust is an effective INP in the free troposphere and has been observed in UT/LS cirrus (Cziczo et al., 2013; Froyd et al., 2010, 2009). A temperature-dependent contact parameter for dust developed by Trainer et al. (2009) for temperatures between 240 and 150 K is used by this nucleation scheme. At warmer temperatures, a constant parameter of 0.97 is used. Note that multiple contact parameters were tested, but 0.97 resulted in the best agreement with observations. We are assuming that every dust particle has the same contact parameter. A more in-depth discussion of these contact parameters can be found in Section 4.1 of this article.

Dust from MAM3 is used for this heterogeneous nucleation parameterization. Dust is treated similarly to sulfates by converting the two-moment representation into a binned distribution for use in CARMA (Figure 1). It is important to note, however, that MAM3 does not track the nearly non-existent Aitken mode dust. Therefore, only accumulation mode and coarse mode dust particles are available for ice nucleation.

The dust core mass within ice crystals and interstitial dust populations are tracked independently within CARMA. However, ice formed via heterogeneous nucleation and ice formed homogeneously are combined together as in situ ice within CARMA. This choice was made in order to reduce the cost of running the model by using fewer advected tracers. In order to distinguish ice formed heterogeneously from ice formed homogeneously, separate runs with and without heterogeneous nucleation were performed.

Prior to the addition of heterogeneous nucleation, CARMA interacted with mixed phase clouds via the freezing of liquid drops and melting of ice, ice crystal growth, and Bergeron processes (Bardeen et al., 2013). The added heterogeneous nucleation scheme now allows CARMA to perform in situ ice nucleation within mixed phase clouds. Therefore, CARMA replaces the default Meyers et al. (1992) mixed phase cloud ice nucleation scheme. The Meyers et al. (1992) ice nucleation scheme performs depositional nucleation onto dust, as well as contact nucleation onto dust based on Young (1974). The remaining liquid microphysics in mixed phase clouds are still handled by the Morrison and Gettelman (2008) scheme.

The authors acknowledge that the heterogeneous nucleation scheme placed into CARMA for this study is limited. This study can be considered as a first order approximation as to how CAM5/CARMA will perform compared to observations with a simple heterogeneous nucleation scheme. Furthermore, a step-by-step approach to developing a heterogeneous nucleation scheme for CARMA allows for the model to be built on a process level and avoid the significant uncertainties associated with other INP.

Future development of heterogeneous nucleation with CARMA should look to incorporate additional ice nucleation pathways, as well as different types of INP in order to capture heterogeneous nucleation over a larger range of conditions and locations. A more comprehensive treatment of contact angle should also be considered. For example, the probability density function approach to contact angle has been shown to lead to a more robust representation of heterogeneous ice nucleation (Y. Wang et al., 2014).

2.5. MAM3 Convective Wet Removal Fix

Recent work by Yu et al. (2019) showed that the wet removal of aerosols within deep convective clouds was inefficient in the CAM/CARMA-aerosol model, because it neglected important physical processes. In brief, the default deep convective cloud scheme in CESM simulates sub-grid scale entrainment and detrainment when it transports aerosols and trace gases within the updraft. However, the in-cloud aerosol wet removal rate is calculated separately from convective transport using grid-box scale quantities. As a result, the CESM convective transport scheme does not consider aerosol activation above cloud base (Berg et al., 2015; H. Wang et al., 2013; Yang et al., 2015) allowing for strong updrafts to transport aerosols upward to 9–18 km in a single time step.

The modified convective transport scheme proposed in Yu et al. (2019) addressed this issue within the CESM1 convective scheme in the following ways: (a) convective scale aerosol-cloud interaction is now treated explicitly following H. Wang et al. (2013); (b) both cloud-borne and interstitial aerosols are convectively transported; (c) an aerosol activation term was added to both the interstitial and cloud-borne aerosol convective transport equations; (d) and, a wet removal term was added to the convective cloud equation. The wet removal term is a function of precipitation rate and in-cloud aerosol mixing ratio.

The present study applies the same Yu et al. (2019) modifications to the CESM1 convective scheme and MAM3 aerosol scheme. The primary difference between Yu et al. (2019) and the present study is the aerosol source. Like CARMA-cirrus, the CARMA-aerosol model is a sectional model, which meant that when applying the Yu et al. (2019) fix to the modes of the MAM3 model, the individual aerosol mass mixing ratio modes had to be treated instead of the binned aerosol distributions. Furthermore, CARMA-aerosol tracks mass mixing ratio and number mixing ratio together while MAM3 tracks them separately. As a result, both were modified to be independent of one another in MAM3.

2.6. The Cloud Feedback Model Intercomparison Project (CFMIP) Observation Simulator Package (COSP)

The CFMIP Observation Simulator Package outputs an alternative set of model fields that allow for a direct comparison with satellite retrievals (Kay et al., 2012). COSP utilizes a number of satellite simulators unique to each instrument onboard a collection of satellites (e.g., MODIS, CALIPSO, CloudSat, etc.). Grid-box means vertical profiles of temperature, humidity, cloud optical thickness, emissivity, and mixing ratios of clouds and precipitation from CAM5 are supplied to each simulator within COSP where instrument-specific models simulate signals and/or retrievals of the satellite instruments (Bodas-Salcedo et al., 2011). As a result, COSP outputs diagnostics similar to the actual observations, thus making them directly comparable to satellite measurements (Bodas-Salcedo et al., 2011).

2.7. Model Dynamics

Specified dynamics (SD) simulations (Lamarque et al., 2011) using MERRA-2 reanalysis data (Gelaro et al., 2017) were performed for all simulations in this study. At the end of each simulation time step the model was nudged toward MERRA-2 reanalysis data by 1% of the difference between the model data and MERRA-2 data. This 1% correction factor was applied to the simulated wind at each model level, as well as latent heat, specific heat, temperature, and surface stresses. All other fields remained unconstrained. Each simulation was conducted at a $1.9° \times 2.5°$ resolution with 72 vertical levels consistent with MERRA-2. SD simulation comparisons with satellite observations occur during the 2006–2008 time period, while comparisons with field missions were simulated over the respective field mission timeframe.

3. Observations Overview

3.1. Aircraft Observations

Dust observations taken by the Particle Analysis by Laser Mass Spectrometry (PALMS, Froyd et al., 2019; Murphy et al., 2006; Thomson et al., 2000) instrument are used to evaluate the simulations of dust in this study. PALMS observes chemical composition of individual particles from approximately 0.1–3 μm size range. PALMS can distinguish between a range of aerosol types and chemical compositions (Froyd et al., 2019; Thomson et al., 2000). Dust and sulfate mass concentration measurements from three missions are used in this study. (a) The Tropical Composition, Cloud, and Climate Coupling (TC^4) mission (Toon et al., 2010) which was centered out of Costa Rica during the fall of 2007, (b) the Mid-latitude Airborne Cirrus Properties Experiment (MACPEX, Jensen, Lawson, et al., 2013) mission which occurred over the Southern United States and Gulf of Mexico during the spring of 2011, and (c) the Studies of Emissions, Atmospheric Composition, Clouds and Climate Coupling by Regional Surveys ($SEAC^4RS$) mission which spanned the continental United States during the fall of 2013 (Toon et al., 2016).

In situ cirrus observations are provided by the 2D-Stereo Optical Array Probe (2D-S, Lawson et al., 2006). The 2D-S probe is a particle shadow-imager that uses two diode laser beams to capture images of ice crystals. Observable ice particles have sizes between approximately 10 μm and 4 mm. 2D-S observations taken by the high altitude aircraft during TC^4 and MACPEX are used here, as well as observations obtained over the Tropical Western Pacific Ocean during the third leg of the Airborne Tropical Tropopause Experiment (ATTREX 3, Jensen et al., 2016).

3.2. Satellite Observations

Simulated large scale ice clouds are evaluated by observations from the Cloud-Aerosol Lidar with Orthogonal Polarization (CALIOP, Vaughan et al., 2005; Winker et al., 2006) instrument onboard the Cloud-Aerosol Lidar and Infrared Pathfinder Satellite Observations satellite (CALIPSO, Winker et al., 2003, 2009). CALIOP is a highly sensitive lidar, capable of observing optically thin cirrus with an observable backscatter limit of ~ 0.001 sr^{-1} that corresponds to a minimum observable extinction limit of 2×10^{-4} km^{-1} (Avery et al., 2012; Winker et al., 2007, 2010). Two CALIPSO products are used in this study. First, cloud fraction observations from the CALIPSO-GOCCP data set (Chepfer et al., 2010) are used to evaluate simulated UT/LS cirrus clouds ($P < 440$ hPa). CALIPSO-GOCCP is a modified CALIPSO data set created to be directly comparable to the

COSP satellite simulator (Section 2.7). The second CALIPSO based data set used in this study is the combined Cloudsat and CALIPSO Ice Cloud Property Product (2C-ICE, Deng et al., 2010, 2013, 2015). One limitation of CALIOP is that the lidar can quickly become attenuated by optically thick clouds. The 2C-ICE data set overcomes this obstacle through the addition of observations from the cloud profiling radar onboard the CloudSat satellite (Stephens et al., 2008). CloudSat, while insensitive to optically thin clouds, is capable of penetrating optically thick clouds, which are common at lower altitudes. By combining these two data sets, 2C-ICE is able to provide a complete atmospheric profile of ice clouds. A $1.9° \times 2.5°$ horizontal resolution was used for both CALIPSO and 2C-ICE data sets. A linear ramp of condensate from 0°C to −10°C was applied to the 2C-ICE data set. This was done in order to remove large peaks in ice water content (IWC) near the melting layer which resulted from water or water-coated ice being observed and interpreted as ice. All condensate is considered to be liquid at temperatures above 0°C, and ice at temperatures less than −10°C (Bardeen et al., 2013). CAM5/CARMA simulations are compared to 2C-ICE observations of cloud fraction, ice water path (IWP), and IWC in this study.

Water vapor observations from the Microwave Limb Sounder (MLS, Waters et al., 2006) and the Atmospheric Infrared Sounder (AIRS, Aumann et al., 2003) are used to evaluate simulated moisture. MLS observations were re-gridded to a $1.9° \times 2.5°$ resolution while AIRS data is on a $1° \times 1°$ resolution.

Observations of cloud radiative forcing are provided by the Clouds and the Earth's Radiant Energy System experiment's Energy Balanced and Filled top of the atmosphere product (CERES-EBAF, Loeb et al., 2018). CERES-EBAF observations are on a $1° \times 1°$ horizontal resolution. All satellite observations have retained their native vertical resolution.

4. Results

4.1. Improved Aerosol Profiles

Before ice nucleation can be studied, we need to ensure that the simulated aerosol fields compare well to observations. Figure 2 shows mission averaged sulfate (top row) and dust (bottom row) vertical profiles for the TC^4 (Figures 2a and 2d), SEAC^{4}RS (Figures 2b and 2e), and MACPEX (Figures 2c and 2f) missions. PALMS observed sulfate profiles that decreased in mass concentration with altitude for all three missions. The primary difference between the missions is the slope of the profile. Also, during SEAC^{4}RS there was an increase in sulfate mass concentration above the 250 hPa altitude level. MACPEX does not have observations near the surface because PALMS was mounted onto the high-altitude WB-57 aircraft, while the instrument was onboard the lower flying DC-8 aircraft during TC^4 and SEAC^{4}RS. As a result, PALMS never sampled air below 700 hPa for MACPEX.

The PALMS observable size range is approximately 0.1–3 μm which encompasses portions of both of the MAM3 coarse and accumulation modes. In order to exclude the influence of particles that fall outside the PALMS observable size range, the fraction of the accumulation and coarse mode which fall within the PALMS size range were computed. This fractional value was then applied to each mode mass respectively.

The simulations shown in Figure 2 are the default simulation profile (green line, CM19 from here on), the simulation with only the Yu et al. (2019) correction (cyan line, Yu19 from here on), the simulation that includes both interactive sulfates and the Yu et al. (2019) correction (purple line, referred to as Hom Nuc from here on), and the simulation which includes interactive sulfates, heterogeneous nucleation, and the Yu et al. (2019) correction (blue line, Het Nuc from here on).

Simulated sulfate profiles in each mission are nearly identical for the CM19, Y19, and Hom Nuc cases at all altitudes below 150 hPa. Only at altitudes above this pressure level do they begin to noticeably differ as the CM19 and Yu19 simulations sulfate mass density decreases at a faster rate than the Hom Nuc simulations. The Het Nuc simulation consistently possesses more sulfate mass than the other three simulations. The largest discrepancy occurs during MACPEX when the Het Nuc simulation has approximately a factor of two more sulfate mass than the other simulations at lower altitudes. All simulations possess too much sulfate mass in each mission, except below 800 hPa in the TC^4 mission and 500 hPa during the SEAC^{4}RS mission.

The slope of the simulated sulfate profiles suggests that sulfate is uniformly mixed and independent of altitude except in the CM19 and Yu19 cases at heights above 200 hPa. Further investigation revealed that the accumulation mode, which dominates the simulated sulfate profile in Figure 2, is the source of this issue (not shown). The fact that the CM19 control case also exhibits this height independence suggests a possible issue with MAM3

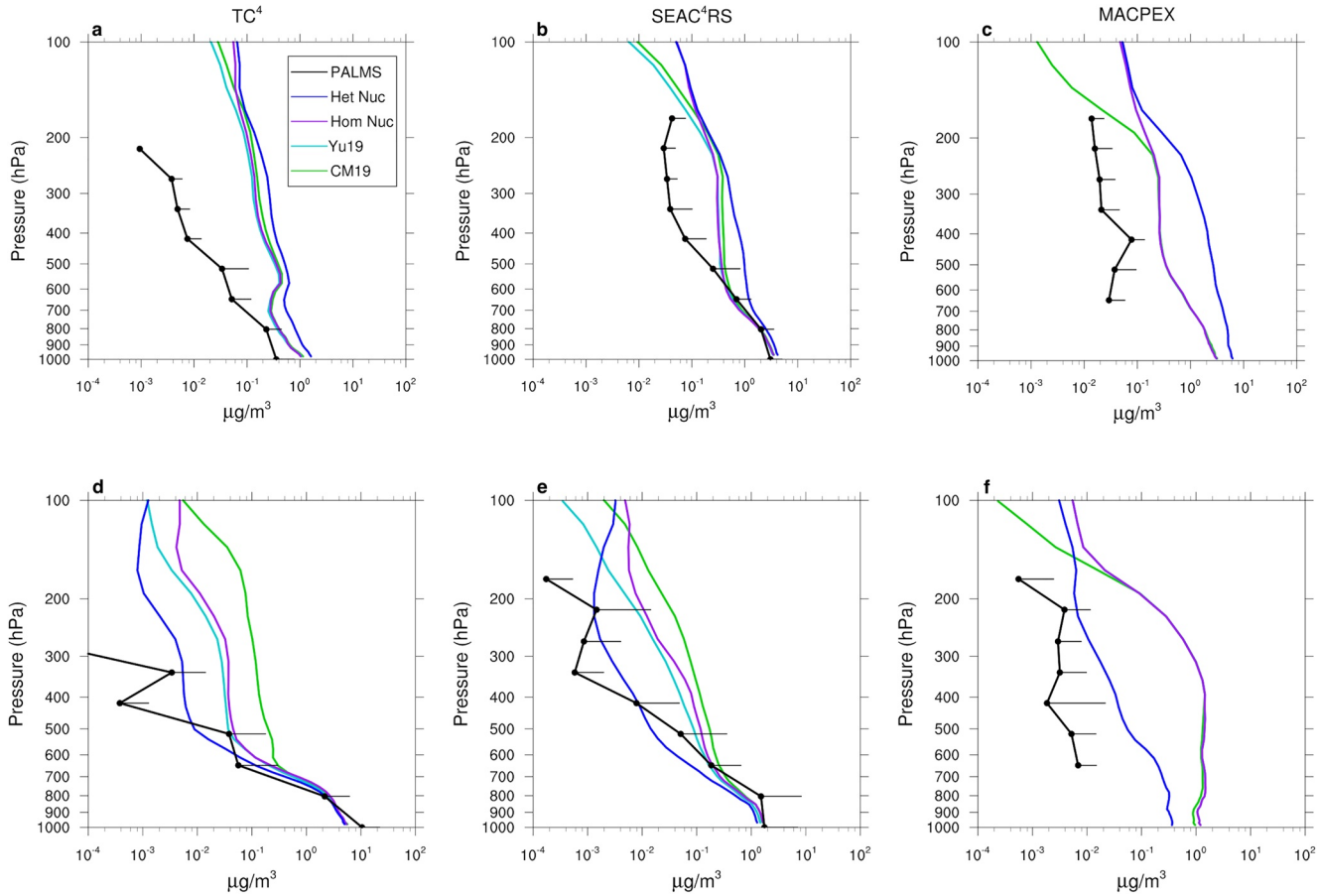

Figure 2. Mission averaged vertical sulfate (top row) and dust (bottom row) mass concentration profiles for the TC^4 (a, d), SEAC^{4}RS (b, e), and MACPEX (c, f) field missions. PALMS observations are represented by the black line with one standard deviation error bars. The CM19, Hom Nuc, and Het Nuc simulations are shown by the green, purple, and blue lines respectively. Size ranges are 0.1–3 microns for TC4 and SEAC4RS and 0.1–1.5 microns for MACPEX.

accumulation mode sulfate and its vertical transport that the Yu et al. (2019) convective fix does not resolve. Liu, Shi, et al., 2012 noted that MAM3 overestimates sulfate over the United States where two of these missions were conducted. Unfortunately, the source of this issue is unclear at this time.

It is interesting that the Het Nuc sulfate profile consistently has more mass compared to the other simulations. The primary difference between the Hom Nuc and Het Nuc cases is the addition of heterogeneous nucleation on dust. The increased sulfate particle mass may be due to MAM's assumption of internally mixed aerosols within each mode. If the concentration of a single aerosol species within a mode significantly changes, it's ratio with other species will also change. This in turn can lead to artificial shifts in the average size of other aerosols within the same mode. In the case presented in Figure 2, dust is drastically reduced through the Yu19 and Het Nuc modifications leading to a reduction in the overall size of aerosols in the coarse mode. Smaller aerosols have longer gravitational settling times and a more persistent higher mass burden. Thus, the sulfate atmospheric mass will increase. This is a problem in MAM first reported by Daniele Visioni of Cornell University that is currently being addressed in a newer version of MAM in CESM2.

The observed dust profiles in the bottom row of Figure 2 are similar in shape for TC^4 and SEAC^{4}RS. Again, low altitude observations are missing from the MACPEX profile. Each PALMS profile shows rapidly decreasing dust mass concentrations as altitude increases until the 300–400 hPa range where the mass concentration is relatively constant for SEAC^{4}RS and MACPEX, or completely disappears (TC^4). The PALMS dust profile then begins decreasing again at approximately 200 hPa.

Simulated dust profiles for TC^4 shows that all four simulations match the observed profile at altitudes below 500 hPa. The Het Nuc profile remains within or on the edge of the upper bound of PALMS observational spread

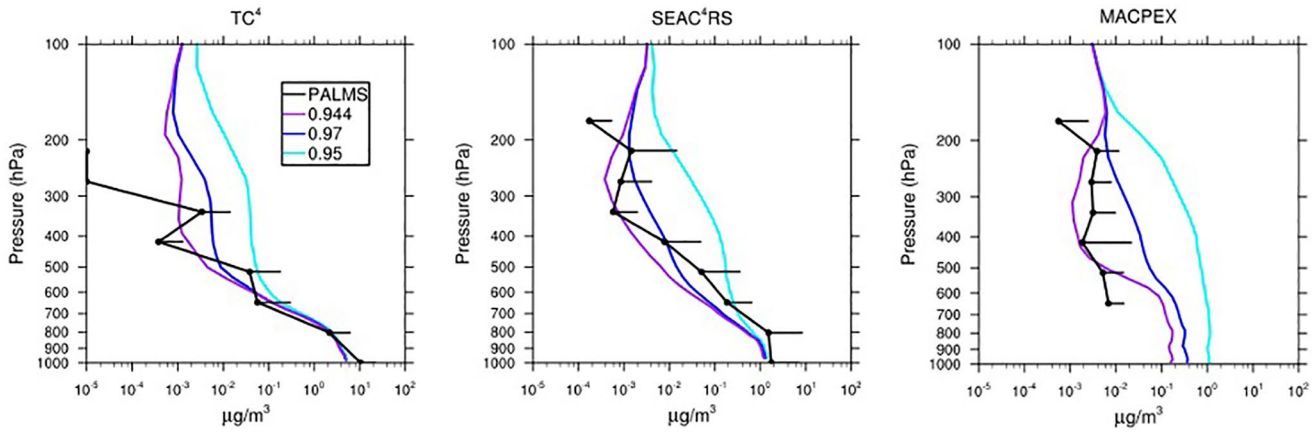

Figure 3. The same as Figure 2 but showing the Het Nuc simulation with three different heterogeneous nucleation contact parameters: (a) 0.95 (cyan), 0.97 (blue), and the Chen et al. (2008) Saharan and Asian dust averaged value (0.994, purple). PALMS observations are again shown in black. The upper bound of observational spread is shown by error bars.

up to 300 hPa where PALMS observations drop off due to unreliable observations. All simulations miss the 400 hPa sudden decrease in dust mass. The default CM19 control case has too much dust mass at all altitudes above 500 hPa.

The simulated SEAC^{4}RS dust profiles produce comparable dust mass to PALMS observations up to 400 hPa. The Het Nuc simulation performs the worst within this altitude range as it is biased low by a factor of 2. Above 400 hPa, the Het Nuc case produces the most comparable profile to PALMS observations while the other cases routinely possess too much dust mass.

Like with the sulfate profile, all four simulations fail to capture the PALMS observed dust profile for the MACPEX mission. Only the Het Nuc case falls within observational error between 300 and 200 hPa. At all other locations, each simulation possesses at least a half order of magnitude too much dust.

Overall, it is evident from Figure 2 that the modifications to the model suggested by Yu et al. (2019), combined with the nucleation changes presented in this study, improve the simulated vertical dust profiles. Simulated dust profiles more closely resemble PALMS observations thanks to a combination of the Yu et al. (2019) convective scavenging fix and the addition of heterogeneous nucleation. Simulated sulfate populations remain largely unaffected by any of the modifications made here, which is expected. However, the simulated sulfate profiles are biased high compared to PALMS measurements.

We experimented with multiple contact parameters for the heterogeneous nucleation scheme. The nucleation rates are very sensitive to the value of the contact parameter. At temperatures warmer than 240 K, three contact parameters were tested, (a) 0.95 which was derived by Wheeler and Bertram (2012) and is often assumed for mineral dust, (b) 0.9945 which is an average of empirically derived contact parameters for Saharan and Asian dust from Chen et al. (2008), and (c) 0.97 which is a midway point between the other two. At temperatures colder than 240 K, the temperature-dependent contact parameter derived for ice clouds by Trainer et al. (2009) is used for all tests. For a solid such as ice, the contact parameter is defined in terms of the surface free energies that for a liquid would determine the angle. Figure 3 shows that these varying contact parameters have different impacts upon simulated dust profiles. The smallest contact parameter (0.95) produces a dust profile with too much mass compared with the observations from each mission. Conversely, the two larger contact parameters each produce a profile which is similar to the PALMS observations; however, it is unclear from Figure 3 which of the two is the more correct assumption. The 0.994 contact parameter produces a dust profile that is similar to the one produced using the 0.97 contact parameter at all levels during TC^4 except at 450 hPa where it captures a portion of the sharp decrease in the observations, but it misses the increase in dust at 350 hPa which the 0.97 contact parameter resolves. The story is similar for the SEAC^{4}RS mission where the 0.97 parameterization is consistently within an order of magnitude of the SEAC^{4}RS observations while the 0.994 simulation has too little dust mass, but catches the decrease in dust at 450 hPa which the 0.97 simulation misses. No parameterization completely

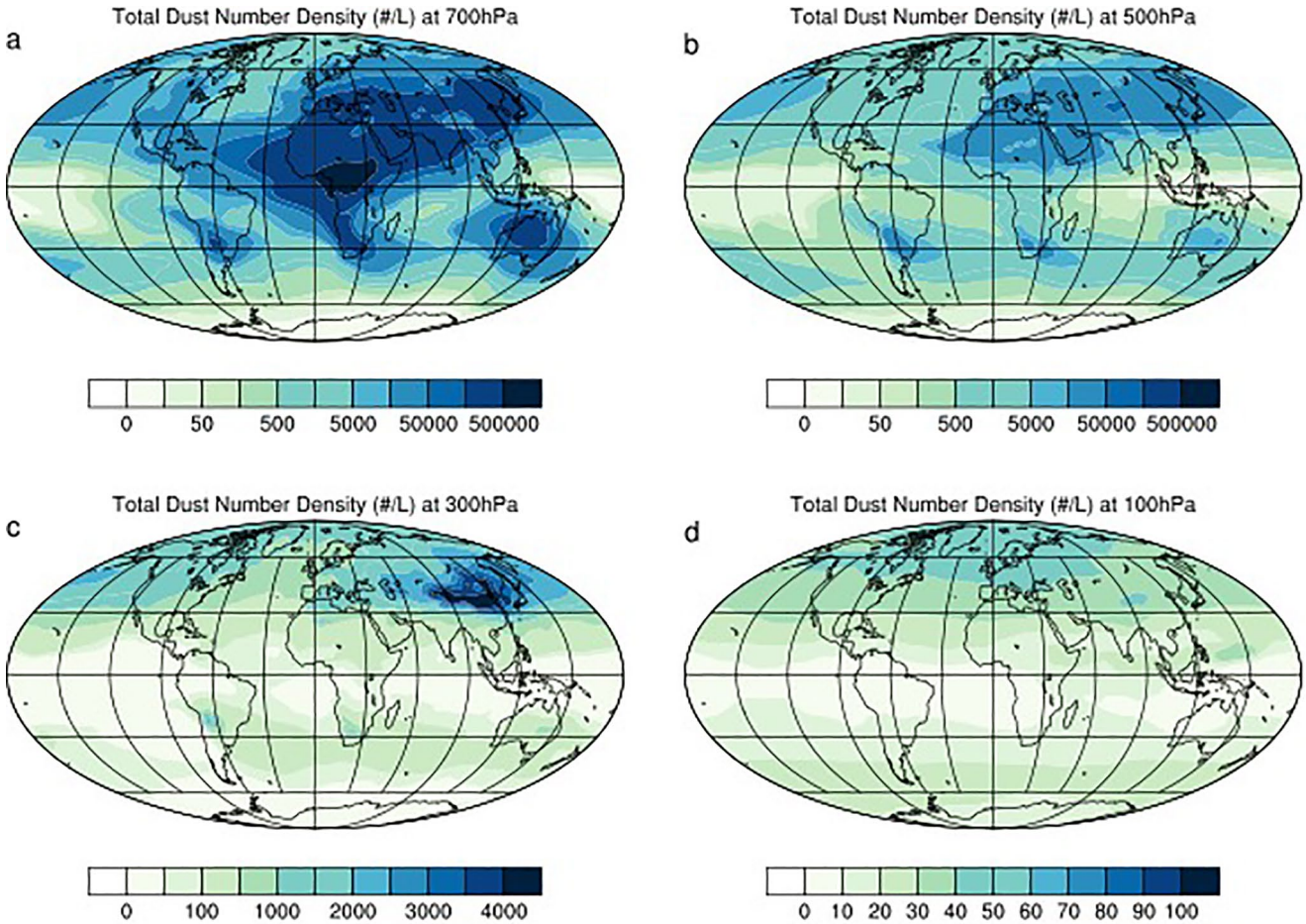

Figure 4. Global dust concentrations in L^{-1} at 700 hPa (a), 500 hPa (b), 300 hPa (c), and 100 hPa (d).

captures the MACPEX profile shape, but the 0.994 contact parameter produces the most comparable profile to PALMS observations.

We opted to use the 0.97 parameterization for three reasons: (a) The 0.97 parameter performed as well as, or better than the other contact parameters during all missions; (b) The 0.97 produced the most comparable dust profile to preliminary PALMS observations from ATOM 1 and 2 (not shown); (c) There were only minor differences in the simulated cloud fields when comparing either the 0.994 contact parameter or the 0.97 contact parameter to satellite observations (not shown).

The global multiyear annual average distribution of dust from the Het Nuc simulation using a 0.97 contact parameter can be seen in Figure 4. The locations of highest dust loading shifts with increasing altitude. Dust is abundant near the surface with the highest concentrations occurring near traditional sources such as the Saharan and Atacama deserts, Central Asia, and Australia (Figure 4a). As one moves to higher altitudes (500 hPa, Figure 4b) the concentration of dust becomes smaller, but the spatial distribution of dust remains the same compared to 700 hPa. Dust concentration continues to decrease at the sub-tropical jet level (300 hPa, Figure 4c) and dust becomes primarily confined to mid and high latitudes (>30°N/S). At 300 hPa the largest dust loading occurs over Asia and the Gobi Desert. This particular region has a strong seasonal signal with high concentrations occurring at 300 hPa during the spring when baroclinic wave activity and dust lifting peaks. Once caught in the jet, dust is transported over most of the northern hemisphere. High dust concentrations persist into the summer months, but become confined over Asia when the Asian Monsoon sets up (not shown). At TTL levels (100 hPa, Figure 4d) dust concentrations have been reduced to <50 L^{-1} globally and are <10 L^{-1} at low latitudes which is consistent with findings from Jensen et al. (2018). The Asian dust signal is still present at 100 hPa.

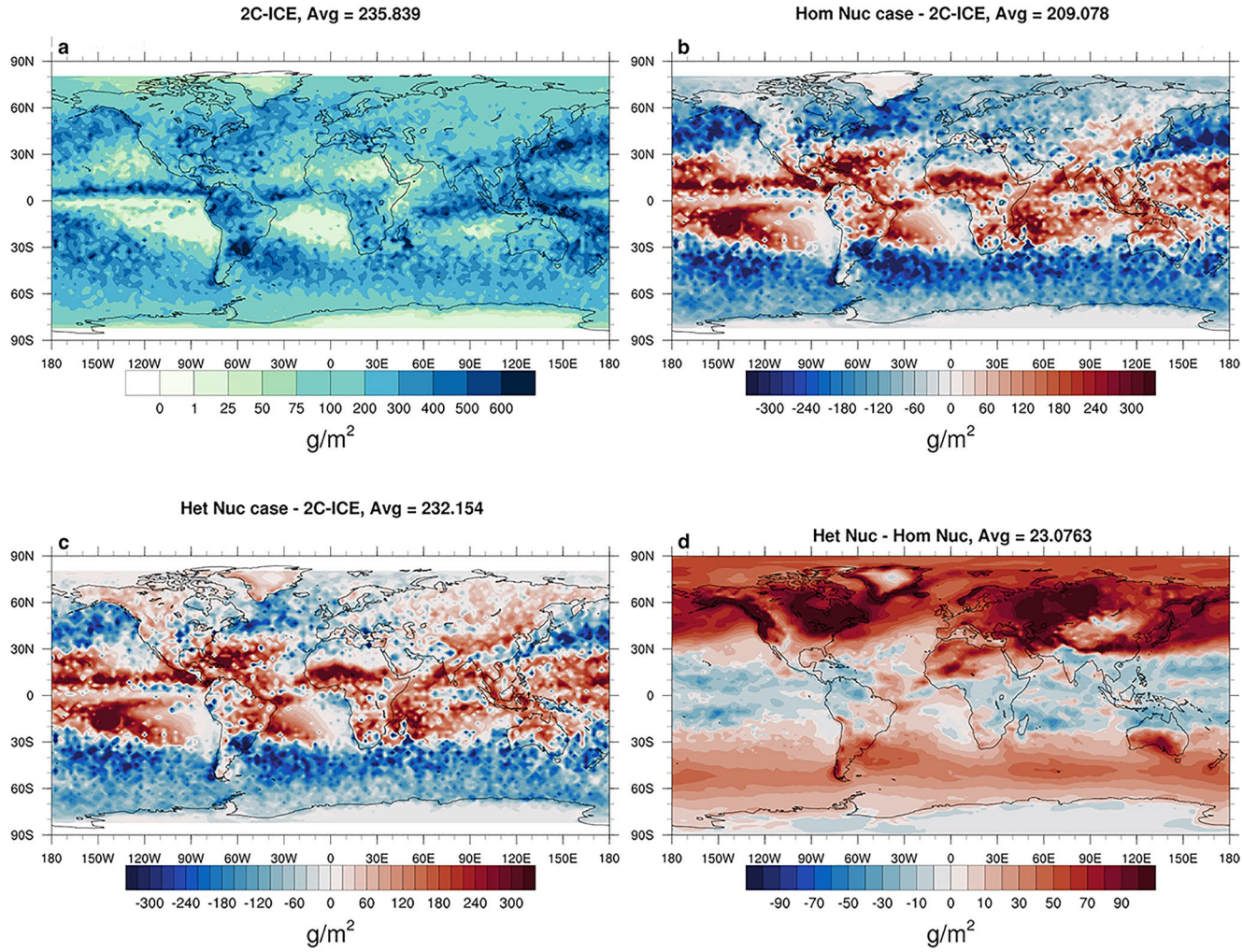

Figure 5. The global distribution of IWP for 2C-ICE observations is shown in panel (a). The difference between the Hom Nuc simulation and 2C-ICE observations (simulation-observations) is shown in panel (b). The difference between the Het Nuc case and 2C-ICE observations is shown in panel (c). Lastly, the difference between model simulations (Het Nuc-Hom Nuc) is shown in panel (d). The value to the right of each title represents the global average.

4.2. Heterogeneous Nucleation Direct Impacts

The direct effects of our CARMA nucleation modifications on the column integrated total in-cloud IWP are shown in Figure 5. 2C-ICE observations show an IWP distribution that reaches a maximum in the tropics where large quantities of cirrus clouds and high-topped convection occur. Other areas of observed elevated IWP occur in the mid-latitude storm tracks and over the Southern Ocean (Figure 5a). The 2C-ICE global IWP average is ~236 g/m^2. Both the Hom Nuc case and the Het Nuc case produce a global IWP distribution that differs from the 2C-ICE observations (Figures 5b and 5c). The tropical IWP in both simulations often exceeds the 2C-ICE observations. The source of the overestimation of tropical IWP is likely the deep convective scheme which is known to both produce too much high cloud over Africa and South America, as well as possess an issue with splitting the Intertropical Convergence Zone (i.e., Delecluse et al., 1998; Lin, 2007; Mechoso et al., 1995; Neelin & Dijkstra, 1995).

Outside of the tropics, where the stratiform cloud model is more important than the deep convection scheme, the Hom Nuc and Het Nuc cases diverge. The Hom Nuc case consistently produces too little IWP in the extra-tropics (Figure 5b). The addition of heterogeneous nucleation improves upon this issue and provides an overall more realistic IWP distribution (Figures 5c and 5d). Compared to the Hom Nuc case, the Het Nuc case produces larger IWP at latitudes poleward of 30°N, most notably over NH landmasses where simulated IWP switches from a deficit to a slight overestimation when compared to 2C-ICE observations (Figures 5b and 5c). Simulated IWP

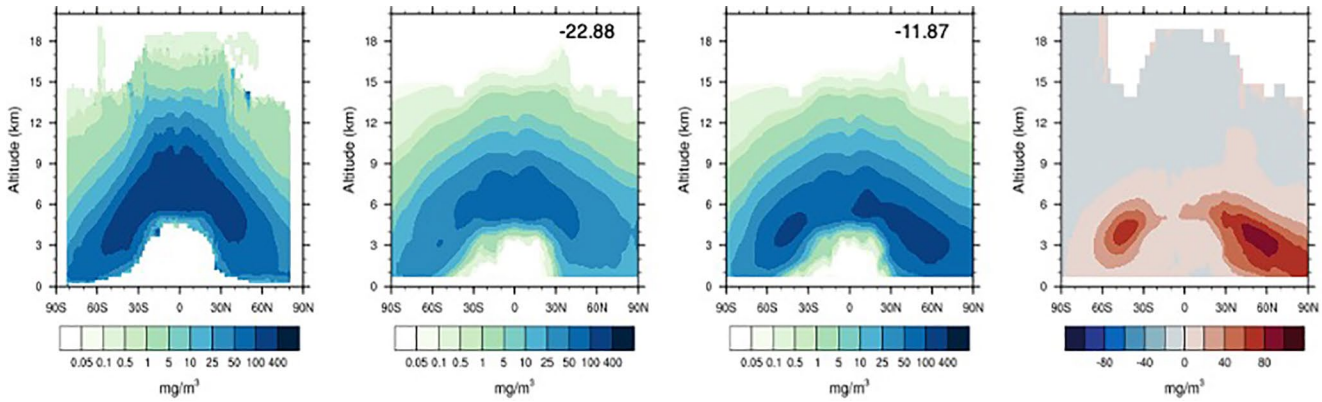

Figure 6. Zonal averages for in-cloud ice water content. From left to right, Figure 6 shows 2C-ICE observations, the Hom Nuc simulation, the Het Nuc simulation, and the difference between the Het Nuc and Hom Nuc simulations (Het Nuc-Hom Nuc). The values in the upper right corner of the simulation zonal averages indicate the (simulation-observation) absolute difference.

also improves over the Southern Ocean where gains of ∼30 g/m^2 occur (Figures 5c and 5d). Furthermore, tropical IWP is reduced when compared to the Hom Nuc case by ∼20 g/m^2 (Figure 5d).

Overall, the addition of heterogenous nucleation in the Het Nuc case reduces the global average IWP bias from 26 g/m^2 in the Hom Nuc case to 3 g/m^2. While the Het Nuc case's global average is closer to the observations, there are canceling overestimates in the tropics and underestimates at higher latitudes.

Another look at the direct effects from the nucleation modifications can be seen in Figure 6, which depicts annual zonal averages of in-cloud IWC. Both simulations possess similar zonal average patterns to the observed in-cloud IWC (Figure 6). The Hom Nuc case underrepresents IWC by ∼22 mg/m^3 on average. The largest discrepancy between the Hom Nuc simulation and 2C-ICE occurs in clouds located between 60°N and 60°S. Within this region 2C-ICE observes clouds with IWC reaching 400 mg/m^3 while the Hom Nuc case consistently has less than 100 mg/m^3 in-cloud. Furthermore 2C-ICE observations see larger ice concentrations at higher altitudes in the tropics.

Between 60°N and 60°S the introduction of heterogeneous nucleation in the Het Nuc case increases the overall simulated zonal IWC distribution by a factor of two. Furthermore, simulated in-cloud IWC almost quadruples in the mid-latitudes reaching concentrations of 400 mg/m^3. The net impact from the introduction of heterogeneous nucleation is a reduction in the zonal average bias by one half. These IWC results agree with the IWP global maps shown in Figure 5, but reveal that much of the improvements can be attributed to warmer, mixed phase ice clouds.

Figure 7 displays vertical profiles of relative humidity (RH) for the tropics (20°S–20°N) and mid-latitudes (20°N/S–60°N/S). Both MLS (top row) and AIRS observations (bottom row) are shown in order to provide a full view of the troposphere and lower stratosphere. Note that AIRS observations use a cloud mask which removes observations with clouds in the pixels and leads to a dry bias. In order to compare simulations with AIRS, the simulations in the bottom row only show clear-sky (ratio of the grid box relative humidity and the cloud free fraction of the model grid box) relative humidity. In the tropics, both simulations are consistently dry by ∼5% above 150 hPa when compared to MLS observations. This is not unexpected as Bardeen et al. (2013) and Maloney et al. (2019) noted that CAM5/CARMA relative humidity is biased low in the TTL. At lower altitudes both simulations are consistently more humid than AIRS observations, especially as one approaches the surface. The introduction of heterogeneous nucleation does little to influence the simulated tropical relative humidity (Figure 7, left column). For most of the simulated tropical RH profile, both simulations are nearly identical. Except at 100 hPa in the TTL where the Het Nuc simulation is about 3% more dry.

The mid-latitudes show a similar relative humidity relationship between observations and simulations as the tropical region (Figure 7, right column). At high altitudes, the simulations are biased low, while at altitudes below 200 hPa the simulations are at least 10% too humid. The addition of heterogeneous nucleation reduces simulated mid-latitude relative humidity by 5%–10% below 250 hPa (Figure 7, bottom right). Figure 6 previously showed

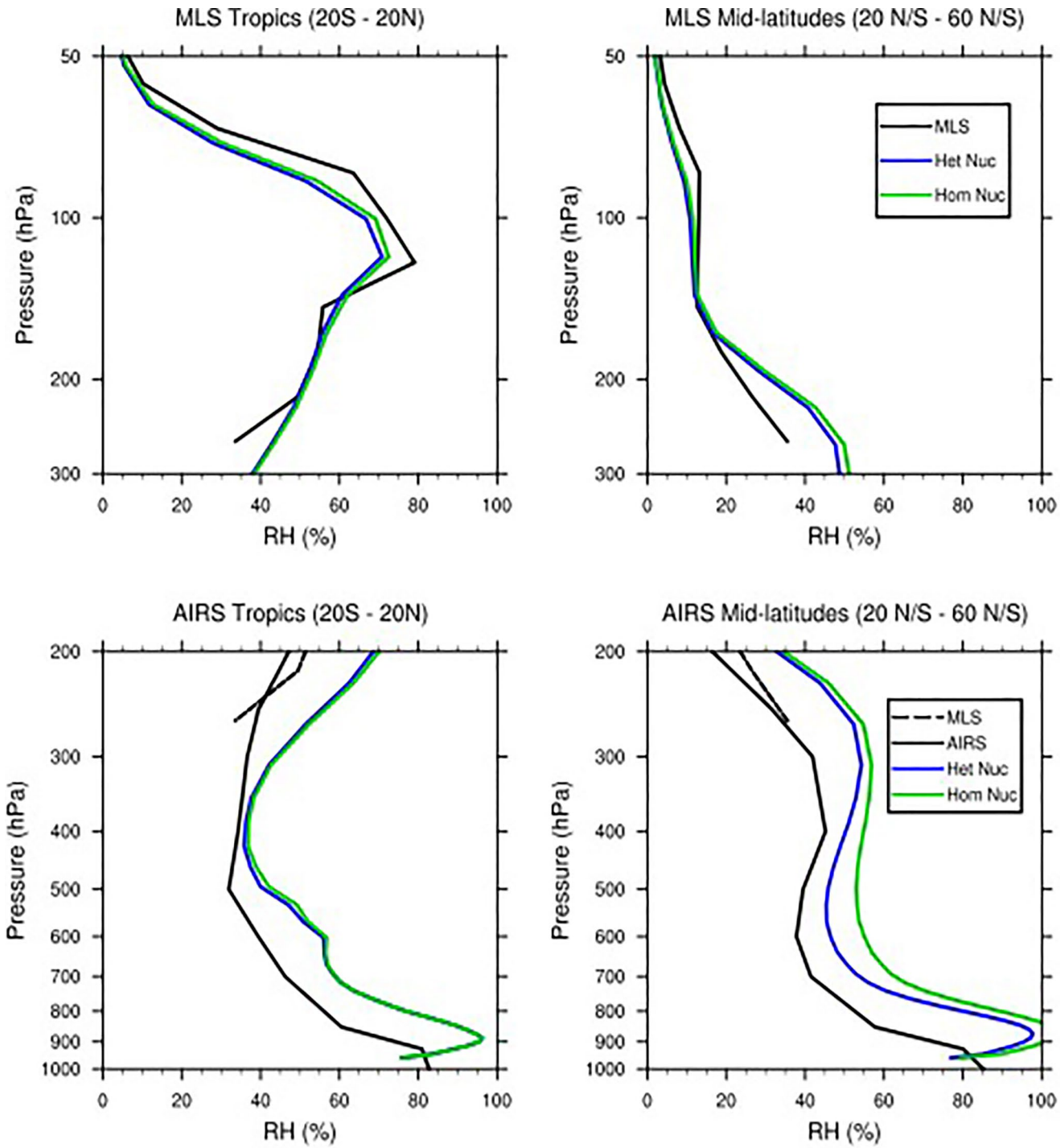

Figure 7. Relative humidity vertical profiles for the tropics (left column) and mid-latitudes (right column). MLS (top row) and AIRS (bottom row) are shown in black alongside the Hom Nuc (green) and the Het Nuc (blue) simulations. MLS data represents the 300–50 hPa altitude range, while AIRS shows data between the surface and 200 hPa. MLS data is also shown as the dashed black line in the overlap region (300–200 hPa) in the AIRS panels. MLS, Microwave Limb Sounder; AIRS, Atmospheric Infrared Sounder.

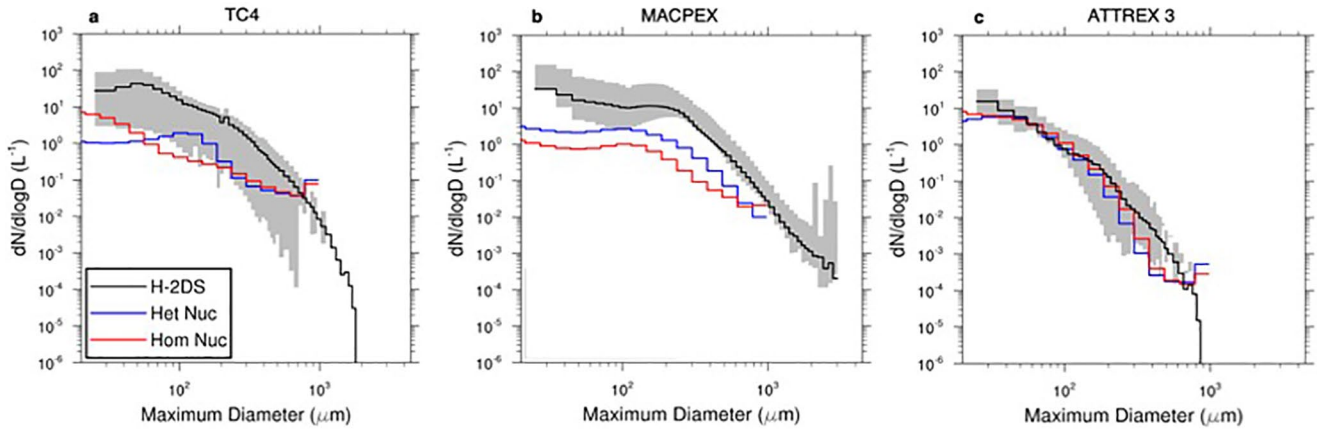

Figure 8. Mission averaged in-cloud ice size distribution for the TC4 (a), MACPEX (b), and ATTREX 3 (c) missions. 2-DS observations are represented by the black line with the 25th–75th quartile range shown in gray. The Hom Nuc (red line) and Het Nuc (blue line) simulations are overlaid on the observational data.

an increase in-cloud IWC due to heterogeneous nucleation on dust occurring within mixed phase clouds. It's likely that the additional in-cloud ice nucleation occurring within mixed phase clouds in the Het Nuc simulation is reducing mid-latitude relative humidity.

Overall, Figure 7 shows that both the Hom Nuc and Het Nuc simulations are often within 5% of the MLS observed RH profile above 200 hPa. At lower levels however, simulated RH is too high when compared to AIRS. The addition of heterogeneous nucleation in the Het Nuc scheme helps lessen this high bias in the mid-latitudes, but the model is still biased higher. A future, more comprehensive heterogenous nucleation scheme in CARMA could help further alleviate this high bias.

4.3. Particle Size Distributions From In-Cloud Observations

In situ observations can provide an in-depth snapshot of conditions inside clouds and reveal if simulated clouds possess the correct number of ice crystals that are properly sized. However, caution must be taken when making such comparisons due to large discrepancies between aircraft observation and model grid-box resolution. In order to simulate aircraft missions successfully, files containing the aircraft's geographical location were used to sample the model along the various mission flight tracks every minute. In the post simulation analysis, a weighted interpolation of the four closest grid-boxes to the aircraft location was performed because the aircraft is not confined to a single grid box or may traverse only a portion of the model grid box in a given time step. As a result, 4 grid cells and two time steps (8 grid cells in total) went into each interpolation to obtain a singular value at the aircraft's location at any given time within a flight. Such steps help alleviate some of the resolution issues associated with comparisons of aircraft data to GCM simulations, but they do not eliminate them. In addition, aircraft often avoid regions with convection at aircraft altitudes, but convection is present in parts of GCM grids.

Figure 8 illustrates in-cloud ice crystal populations obtained from aircraft flights. High altitude in-cloud ice crystal size distributions observed by the 2D-S instrument are shown for the TC^4 (panel a), MACPEX (panel b), and ATTREX 3 (panel c) missions. In each mission, the lower limit for 2D-S measurements of ice crystals was 20 μm. The observed maximum-sized ice crystal varies from mission to mission, however. MACPEX encountered the largest ice crystals (3,000 μm) while ATTREX 3 observed the smallest crystals, with no ice crystal exceeding 900 μm in size.

Each simulation shown in Figure 8 is the in situ ice size distribution. The Hom Nuc case in Figure 8 (red line) lies within the TC^4 observational spread between 20 and 30 μm and between 200 and 800 μm sized particles. Between 30 and 200 μm the Hom Nuc case has too few particles. The MACPEX Hom Nuc case also has too few simulated ice crystals when compared to 2DS observations. Finally, the Hom Nuc case compares well to ATTREX 3 observations as it consistently falls within observational spread. Of note, both TC^4 and ATTREX 3 simulations overestimate the observed ice concentration in the largest size bin where the distribution plateaus. The cause

of this plateau at the largest sizes is due to CARMA's upper in situ ice boundary. Any simulated ice larger than 900 μm will be put into the largest size bin. Furthermore, CARMA converts its largest size bin into snow. Snow is allowed to precipitate over multiple time step s instead of being removed at the end of each time step (Bardeen et al., 2013). This results in snow remaining aloft longer, continuously populating the largest size bin.

The inclusion of heterogeneous nucleation impacts the simulated ice size distribution differently in each mission (Figure 8, blue line). During the TC^4 mission, the inclusion of heterogeneously active dust lowered the concentration of smaller ice crystals (<40 μm) when compared to the Hom Nuc case, but increased the amount of simulated in cloud ice by a half order of magnitude between 40 and 200 μm which now falls within observational spread within this range. At larger sizes than 200 μm both simulations are similar to one-another. The impact on the ice crystal size distribution for MACPEX is an overall increase in ice concentration across all sizes by a factor of two, but the Het Nuc case still possess too little ice when compared to observations. The ATTREX 3 simulations produced identical distributions for small particles (<100 μm), but the Het Nuc case is consistently a half order of magnitude lower than the Hom Nuc case for large ice particles. However, it still falls within the lower limit of the observational spread.

While viewing these in-cloud size distributions it is important to consider the regions and types of clouds sampled. In TC^4 and MACPEX the clouds would largely have been generated by detrained ice. TC^4 was based in Costa Rica and flights occurred primarily over the ocean in the extensive anvils of mesoscale convection. Almost no flights occurred in stratiform clouds which formed in situ, instead most were dominated by detrained ice. MACPEX flights occurred over the southern United States and the Gulf of Mexico and primarily sampled ice from anvils. ATTREX 3 was based in Guam and surveyed the Tropical Western Pacific. In ATTREX3, the Global Hawk aircraft avoided convective clouds, and are the least contaminated by detrained ice. Both TC^4 and MACPEX occurred in regions where Saharan dust is commonly found, while the Tropical Western Pacific is a generally pristine region (Figure 4). As a result, the addition of heterogeneously nucleating dust aerosols will impact each region differently. For example, TC^4 and MACPEX spent some time sampling cirrus that were in the outflow from Saharan dust which may be why both simulation's in-cloud ice size distributions change when heterogeneous nucleation is included. Conversely, ATTREX 3 rarely encountered heterogeneously formed cirrus, which it is why there are little to no changes in the size distribution when heterogeneous nucleation is included. Had ATTREX 3 occurred during the Northern Hemisphere summer when the Asian Monsoon was at peak strength, the in-cloud ice concentrations might look different.

From Figure 8, we can conclude that the addition of dust as an INP in the CARMA-cirrus model helps improve the concentration of mid-size to large ice crystals (>30 μm) in regions where dust is present; however, it is unclear from Figure 8 if there is a positive or negative impact upon smaller ice crystal concentrations. Possibly the model needs to include additional types of heterogeneous nuclei, such as sea salt, organics, and black carbon so that the number of ice particles goes up, and their mean radius goes down relative to observations (Hoose et al., 2010; Hoose & Möhler, 2012).

4.4. Nucleation Indirect Effects

Heterogeneous nucleation could produce indirect effects on cloud fraction and radiative transfer. Cloud fraction in CAM5/CARMA is dependent upon relative humidity and IWC, while the model's radiative transfer code is dependent upon cloud fraction, as well as particle size and IWP. Therefore, changes to ice nucleation should have a downstream impact upon these two important model fields. It should be noted that sub-grid scale cloud fraction is not physically based, but instead found from empirical parameterizations.

The left panel in Figure 9 illustrates annual zonal average cloud fraction retrieved by 2C-ICE observations. On average, the Hom Nuc and Het Nuc simulations under represent zonal cloud fraction by approximately 1.8% and 2.3% respectively. In the tropics and UT/LS, both simulations produce zonal cloud fractions which resemble the 2C-ICE observations in both spatial distribution and magnitude (middle two panels of Figure 9). However, both simulations produce too few clouds at higher latitudes in the free troposphere. The far-right panel in Figure 9 shows the difference in cloud fraction between the Het Nuc and Hom Nuc simulations. Here it is evident that the introduction of our basic heterogeneous nucleation scheme produces less mid-latitude clouds.

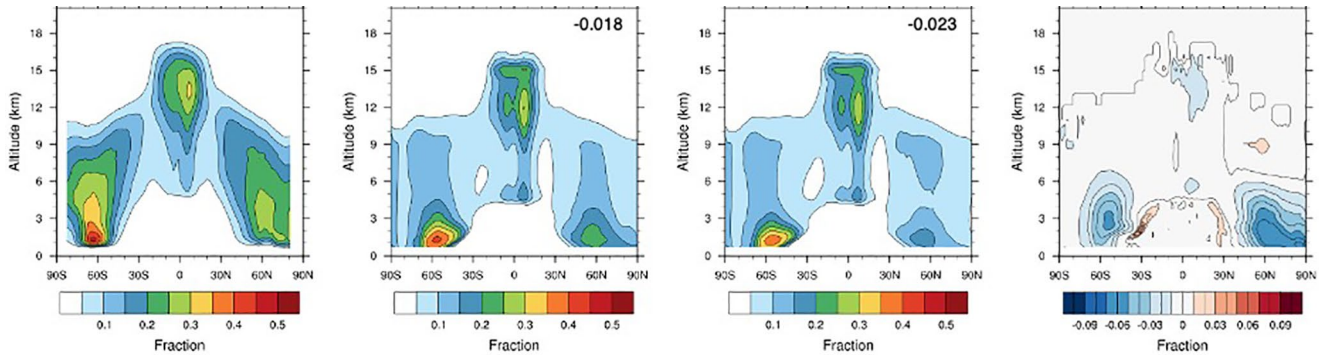

Figure 9. Annual average zonal cloud fraction. From left to right, Figure 9 shows 2C-ICE observations, the Hom Nuc case, the Het Nuc case, and the difference between the Het Nuc and Hom Nuc cases (Het Nuc-Hom Nuc). The values in the upper right corner of the simulation zonal averages indicate the (simulation-observation) absolute difference.

The global average COSP simulated high cloud fraction (clouds at pressures <440 hPa) and the ice cloud sensitive long wave cloud forcing (LWCF) are biased low by ∼13.5% and ∼10 W/m^2 respectively when compared to CALIPSO-GOCCP and CERES-EBAF observations (not shown). However, both the Hom Nuc and Het Nuc simulations produce nearly identical results. Taken with the in-cloud ice crystal size distributions from Figure 8, these results suggest that this basic heterogeneous nucleation scheme has a minor impact on high cirrus clouds.

5. Discussion

The results presented above make evident that the choice to use interactive sulfates versus a fixed sulfate climatology had little impact on the simulated ice cloud fields. Conversely, the inclusion of heterogeneous nucleation of ice on dust aerosols provides improved simulations of IWP, IWC, and improved concentrations of moderately to large-sized ice crystals. The greatest impacts occur at lower altitudes where mixed phase clouds form and in the mid-latitude regions where dust is abundant.

There is a clear division in the CAM5/CARMA model simulated cirrus clouds as to where heterogeneous nucleation and homogeneous nucleation dominate. This separation can be seen in Figure 10, which shows the zonally averaged fractional occurrence of heterogeneous nucleation (colored contours) and homogeneous nucleation (line contours) for stratiform clouds during the multiyear simulation. A mask has been applied to the zonal average in Figure 10 to only show in-cloud ice rather than grid cell average ice. Figure 10 shows that homogeneous nucleation only occurs at temperatures colder than 240 K (red line). At altitudes below this temperature line, heterogeneous nucleation is frequent. This relationship is not unexpected as the Koop et al. (2000) scheme used for homogeneous nucleation in CARMA only begins nucleating ice at temperatures ≤240 K. However, another part of the prevalence of homogeneous nucleation at cold temperatures is that very few dust particles reach those altitudes, except for high northern latitudes. We have already shown in Figures 2 and 3 that prior to the work of Yu et al. (2019), many simulations likely greatly overestimated the amount of dust at high altitudes and therefore overestimated the amount of heterogeneous nucleation.

An interesting take away from Figure 10 is that in the TTL, there is little to no signal from heterogeneous nucleation. An ongoing debate within the scientific community concerns the importance of heterogeneous nucleation within the TTL. Previous studies have shown that dust is present and is an active INP in the TTL (e.g., Cziczo et al., 2013; Froyd et al., 2010). However, other studies have shown that dust, while an important INP in the free troposphere, is too scarce in the TTL and is an ineffective INP at TTL temperatures (e.g., Froyd et al., 2009; Jensen et al., 2018). Figure 10 supports the latter hypothesis as there is little to no heterogeneous nucleation occurring in the TTL in our model. However, this study only includes vapor deposition on dust. There may be other types of heterogeneous nuclei, such as black carbon and glassy organic aerosols. Also, dust can trigger the nucleation of liquid aerosols by immersion nucleation, which is not included in the modifications made to CAM5/CARMA in this study. The other results from this study further support the case against TTL dust serving as the

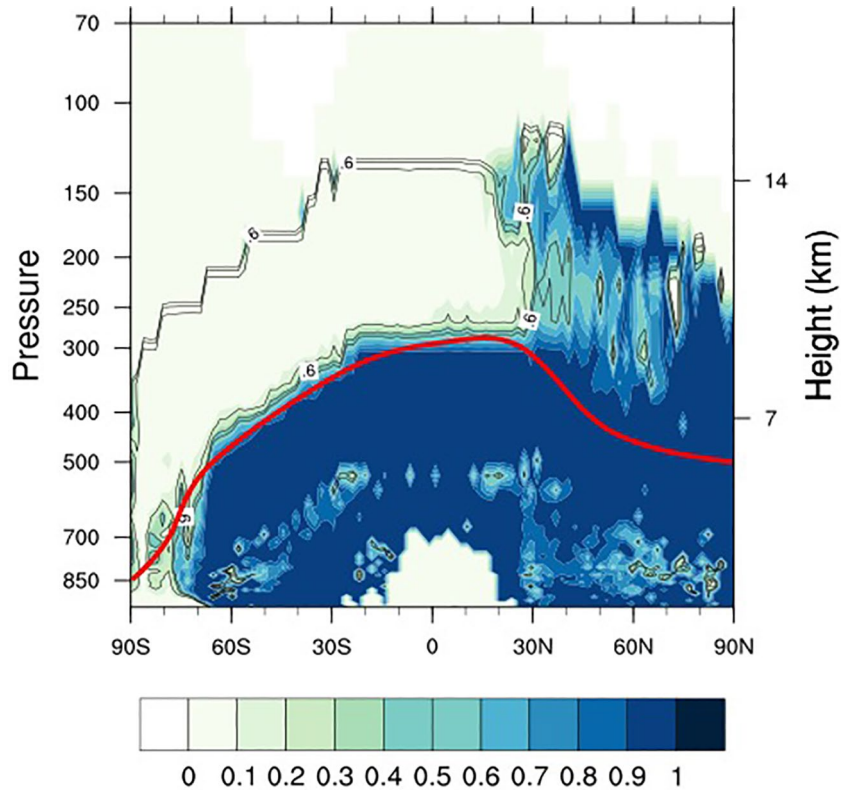

Figure 10. A zonal average of the fractional occurrence of in-cloud heterogeneously nucleated ice (colored contours) and homogeneously nucleated ice (numbered contours). The red line shows the simulated 240 K isotherm.

primary INP. For example, it was shown that simulated TTL dust is sparse (<10 L^{-1}, Figure 4) and that TTL cloud fraction is relatively insensitive to the addition of heterogeneous nucleation (Figure 9).

North of 30°N and for altitudes above 7 km, Figure 10 shows a mixture of heterogeneous nucleation and homogeneous nucleation. Poleward of 30°N the fractional occurrence of ice nucleation attributed to heterogeneous nucleation often exceeds 0.5 and occurs more frequently than homogeneous nucleation. Located in this latitude band is the region of high dust concentrations above 300 hPa associated with lofting from baroclinic wave activity and the Asian Monsoon.

All of these results point to the importance of including heterogeneous nucleation in simulations of ice clouds within the CARMA sectional ice cloud model. Dust has a noticeable impact upon middle troposphere ice clouds, but a more suitable INP should be considered for high ice clouds. Previous work (e.g., Abbatt et al., 2006; Jensen et al., 2018) has suggested effloresced ammonium sulfate as a potential candidate as ammoniated sulfates are the most common aerosol in the troposphere, though organo-sulfates, glassy organics, and nitrates can also be abundant.

Lastly it is important to consider the impact that the CARMA heterogeneous nucleation scheme has on mixed phase clouds. The greatest change to simulated clouds occurred in in-cloud IWC, IWP, and cloud fraction at mid-to-lower altitudes in mid-latitude mixed phase clouds. In these regions, in-cloud IWC, IWP both increased which suggests more ice nucleation within mixed phase clouds (Figures 5 and 6); however, cloud fraction and relative humidity in these areas decreased (Figures 7 and 9). Therefore, it can be surmised that the heterogeneous nucleation scheme added to CARMA nucleates dust too efficiently, resulting in more ice nucleation within fewer mixed phase clouds that deplete the surrounding air of moisture more strongly.

As it was previously mentioned, this heterogeneous nucleation scheme is intentionally limited in scope in order to provide a first test of CARMA's capabilities of performing heterogeneous nucleation. The results shown in this study unsurprisingly show that a more realistic nucleation scheme is needed. Future iterations of this scheme

could be improved by the inclusion of more heterogeneous nucleation pathways such as immersion and condensation freezing, a more flexible PDF representation of dust contact angles, as well as additional INP species.

6. Summary and Future Work

Modifications to the treatment of aerosols and nucleation of ice within the CAM5/CARMA model were evaluated in this study. The first modification was the addition of the techniques of Yu et al. (2019) to the convective transport of aerosols. The second was a switch from the English et al. (2011) sulfate climatology to an interactive sulfate field provided by the MAM3 model. The final modification was the introduction of a basic heterogeneous ice nucleation scheme for water vapor deposition on dust, which uses MAM3 supplied dust as INP. It is assumed that the number of dust particles present in a MAM3 mode is proportional to its mass fraction in the mixed aerosols. The implementation of these three changes resulted in a dust aerosol profile similar to PALMS observations from numerous field missions (Figures 2 and 3).

Simulations with the improved aerosol field and Yu et al. (2019) correction were evaluated with satellite observations from CALIPSO, CloudSat, CERES, MLS, and AIRS, as well as in situ 2-DS and PALMS observations from a number of field missions. The interactive sulfates provided little change from the previously used cloud climatology. However, the model produces more sulfate than observed in the upper troposphere in several field missions. If this is a global problem, it may be biasing the homogeneous nucleation of ice. The inclusion of heterogeneous nucleation improves simulated IWC in the mid-to-lower troposphere and the size distribution of ice crystals larger than 30 μm. IWP responded strongly to the inclusion of heterogeneous nucleation with a reduction of ∼20 g/m^2 occurring in the tropics and an increase in IWP ranging from 100 to 200 g/m^2 at higher latitudes.

Cloud fraction is only indirectly impacted by cloud physics in the CESM1 model, and is based on empirical parameterizations rather than physically based parameterizations. The inclusion of heterogeneous nucleation caused only small changes in high cloud fraction by reducing simulated ice cloud fraction by <10%, because few dust particles are found in the upper troposphere. Due to the insensitivity of high cloud fraction to heterogeneously active dust, LWCF forcing remained relatively unchanged when heterogeneous nucleation was included. Instead, heterogeneous nucleation impacts mid-troposphere to low troposphere in-cloud ice crystal concentrations and the local relative humidity. Other INP candidates, mainly produced as secondary aerosols such as ammoniated sulfate and organo-sulfates, may produce a stronger signal in high ice clouds than dust.

While the results presented in this study show improvements to some simulated ice cloud fields within the CAM5/CARMA model, further work is still needed. Additional testing with heterogeneous nucleation is needed in the CARMA-cirrus model. The parameterization presented here is limited by the use of only one type of INP and one mode of nucleation of potentially many. Other studies have suggested viable candidates for INP, such as effloresced ammonium sulfate in the TTL. A potential, more significant improvement in cloud simulations would be to move to CESM2. The Morrison and Gettelman (2008) liquid cloud model include immersion nuclei in CESM2, and is used for both stratiform and shallow convective clouds. Lastly, one final way to improve the representation of ice clouds within GCM's is to increase GCM grid-box resolution. This will greatly reduce the reliance upon cloud parameterizations of cloud fraction as more physical processes can be resolved.

Data Availability Statement

CAM5/CARMA model output is open to the public and stored at osf.io/wq6bv (https://doi.org/10.17605/OSF.IO/WQ6BV). The ATTREX 3, TC^4, and MACPEX aircraft data used in this study is open to the public and can be found on the NASA Earth Science Project website (espoarchive.nasa.gov). SEAC^{4}RS data can be found at the NASA Airborne Science for Atmospheric Composition website (https://www-air.larc.nasa.gov/missions/seac4rs/index.html). The PALMS data for each field mission can be found at espoarchive.nasa.gov and at osf.io/wq6bv (https://doi.org/10.17605/OSF.IO/WQ6BV). The authors would like to express gratitude for all of the hard work done by the instrument teams involved in each mission and for making their data accessible. CERES-EBAF data used in this study can be obtained from the NASA Langley Research Center Atmospheric Science Data Center (asdc.larc.nasa.gov) while the CALIPSO-GOCCP data set can be obtained from the ClimServ CFMIP web page (https://climserv.ipsl.polytechnique.fr/cfmip-obs/Calipso_goccp.html). AIRS, MLS, and MERRA 2 data can be found at the NASA Goddard Earth Sciences data repository (disc.gsfc.nasa.gov).

Acknowledgments
The work performed here was supported by the NSF Climate and Large-Scale Dynamics Program AGS1640903 Grant. The authors would like to acknowledge high-performance computing support from Cheyenne (https://doi.org/10.5065/D6RX99HX) provided by NCAR's Computational and Information Systems Laboratory, sponsored by the National Science Foundation. The authors of this article would like to thank Daniel Visioni of Cornell University for his discovery and guidance navigating the MAM aerosol issue. The authors would also like to acknowledge the contributions of Bruce Anderson, Lee Thornhill, and Luke Ziemba (NASA Langley Research Center) for aerosol size distribution measurements during TC^4 and $SEAC^4RS$, as well as James Wilson (Denver University) for size distribution measurements during MACPEX.

References

Abbatt, J. P. D., Benz, S., Cziczo, D. J., Kanji, Z., Lohmann, U., & Möhler, O. (2006). Solid ammonium sulfate aerosols as ice nuclei: A pathway for cirrus cloud formation. *Science*, *313*, 1770–1774. https://doi.org/10.1126/science.1129726

Aumann, H. H., Chahine, M. T., Gautier, C., Goldberg, M. D., Kalnay, E., Mcmillin, L. M., et al. (2003). AIRS/AMSU/HSB on the Aqua mission: Design, science objectives, data products, and processing systems. *IEEE Transactions on Geoscience and Remote Sensing*, *41*(2), 253–264. https://doi.org/10.1109/TGRS.2002.808356

Avery, M., Winker, D., Heymsfield, A., Vaughan, M., Young, S., Hu, Y., & Trepte, C. (2012). Cloud ice water content retrieved from the CALIOP space-based lidar. *Geophysical Research Letters*, *39*. https://doi.org/10.1029/2011GL050545

Bardeen, C. G., Gettelman, A., Jensen, E. J., Heymsfield, A., Conley, A. J., Delanoë, J., et al. (2013). Improved cirrus simulations in a general circulation model using CARMA sectional microphysics. *Journal of Geophysical Research: Atmospheres*, *118*, 11679–11697. https://doi.org/10.1002/2013JD020193

Bardeen, C. G., Toon, O. B., Jensen, E. J., Marsh, D. R., & Harvey, V. L. (2008). Numerical simulations of the three-dimensional distribution of meteoric dust in the mesosphere and upper stratosphere. *Journal of Geophysical Research*, *113*. https://doi.org/10.1029/2007JD009515

Berg, L. K., Shrivastava, M., Easter, R. C., Fast, J. D., Chapman, E. G., Liu, Y., & Ferrare, R. A. (2015). *A new WRF-Chem treatment for studying regional-scale impacts of cloud processes on aerosol and trace gases in parameterized cumuli* (Vol. 2013, pp. 409–429). Geoscientific Model Development. https://doi.org/10.5194/gmd-8-409-2015

Bodas-Salcedo, A., Webb, M. J., Bony, S., Chepfer, H., Durfresne, J. L., Klein, S. A., et al. (2011). COSP: Satellite simulation software for model assessment. *Bulletin of the American Meteorological Society*, *92*, 1023–1043. https://doi.org/10.1175/2011BAMS2856.1

Chen, J., Hazra, A., & Levin, Z. (2008). Parameterizing ice nucleation rates using contact angle and activation energy derived from laboratory data. *Atmospheric Chemistry and Physics*, *8*, 7431–7449. https://doi.org/10.5194/acp-8-7431-2008

Chepfer, H., Bony, S., Winker, D., Cesana, G., Dufresne, J. L., Minnis, P., et al. (2010). The GCM-oriented CALIPSO cloud product (CALIPSO-GOCCP). *Journal of Geophysical Research: Atmospheres*, *115*(5). https://doi.org/10.1029/2009JD012251

Comstock, J. M., Ackerman, T. P., & Mace, G. G. (2002). Ground-based lidar and radar remote sensing of tropical cirrus clouds at Nauru Island: Cloud statistics and radiative impacts. *Journal of Geophysical Research: Atmospheres*, *107*(23), AAC 16-1–AAC 16-14. https://doi.org/10.1029/2002JD002203

Corti, T., Luo, B. P., Fu, Q., Vömel, H., & Peter, T. (2006). The impact of cirrus clouds on tropical troposphere-to-stratosphere transport. *Atmospheric Chemistry and Physics*, *6*, 1725–1747. https://doi.org/10.5194/acpd-6-1725-2006

Cziczo, D. J., Froyd, K. D., Hoose, C., Jensen, E. J., Diao, M., Zondlo, M. A., et al. (2013). Clarifying the dominant sources and mechanisms of cirrus cloud formation. *Science*, *340*(6138), 1320–1324. https://doi.org/10.1126/science.1234145

Delecluse, P., Davey, M. K., Kitamura, Y., Philander, S. G. H., Suarez, M., & Bengtsson, L. (1998). Coupled general circulation modeling of the tropical Pacific. *Journal of Geophysical Research: Oceans*, *103*(C7), 14357–14373. https://doi.org/10.1029/97jc02546

Demott, P. J., Prenni, A. J., Liu, X., Kreidenweis, S. M., Petters, M. D., Twohy, C. H., et al. (2010). Predicting global atmospheric ice nuclei distributions and their impacts on climate. *Proceedings of the National Academy of Sciences of the United States of America*, *107*(25), 11217–11222. https://doi.org/10.1073/pnas.0910818107

Deng, M., Mace, G. G., Wang, Z., & Berry, E. (2015). CloudSat 2C-ICE product update with a new Z_e parameterization in lidar-only region. *Journal of Geophysical Research: Atmospheres*, *12*, 198–208. https://doi.org/10.1002/2015JD023600.Received

Deng, M., Mace, G. G., Wang, Z., & Lawson, R. P. (2013). Evaluation of several A-Train ice cloud retrieval products with in situ measurements collected during the SPARTICUS campaign. *Journal of Applied Meteorology and Climatology*, *52*, 1014–1030. https://doi.org/10.1175/JAMC-D-12-054.1

Deng, M., Mace, G. G., Wang, Z., & Okamoto, H. (2010). Tropical composition, cloud and climate coupling experiment validation for cirrus cloud profiling retrieval using CloudSat radar and CALIPSO lidar. *Journal of Geophysical Research*, *115*. https://doi.org/10.1029/2009JD013104

Easter, R. C., Ghan, S. J., Zhang, Y., Saylor, R. D., Chapman, E. G., Laulainen, N. S., et al. (2004). MIRAGE: Model description and evaluation of aerosols and trace gases. *Journal of Geophysical Research*, *109*. https://doi.org/10.1029/2004JD004571

English, J. M., Toon, O. B., Mills, M. J., & Yu, F. (2011). Microphysical simulations of new particle formation in the upper troposphere and lower stratosphere. *Atmospheric Chemistry and Physics*, *11*(17), 9303–9322. https://doi.org/10.5194/acp-11-9303-2011

Froyd, K. D., Murphy, D. M., Brock, C. A., Campuzano-Jost, P., Dibb, J. E., Jimenez, J. L., et al. (2019). A new method to quantify mineral dust and other aerosol species from aircraft platforms using single-particle mass spectrometry. *Atmospheric Measurement Techniques*, *12*(Issue 11), 6209–6239. https://doi.org/10.5194/amt-12-6209-2019

Froyd, K. D., Murphy, D. M., Lawson, P., Baumgardner, D., & Herman, R. L. (2010). Aerosols that form subvisible cirrus at the tropical tropopause. *Atmospheric Chemistry and Physics*, *10*, 209–218. https://doi.org/10.5194/acp-10-209-2010

Froyd, K. D., Murphy, D. M., Sanford, T. J., Thomson, D. S., Wilson, J. C., Pfister, L., et al. (2009). Aerosol composition of the tropical upper troposphere. *Atmospheric Chemistry and Physics*, *9*, 4363–4385. https://doi.org/10.5194/acp-9-4363-2009

Fueglistaler, S., Dessler, A. E., Dunkerton, T. J., Folkins, I., Fu, Q., & Mote, P. W. (2009). Tropical tropopause layer. *Review of Geophysics*, *47*. https://doi.org/10.1029/2008RG000267

Gelaro, R., McCarty, W., Suárez, M. J., Todling, R., Molod, A., Takacs, L., et al. (2017). The modern-era retrospective analysis for research and applications, version 2 (MERRA-2). *Journal of Climate*, *30*(14), 5419–5454. https://doi.org/10.1175/jcli-d-16-0758.1

Heymsfield, A. J., Schmitt, C., Bansemer, A., & Twohy, C. H. (2010). Improved representation of ice particle masses based on observations in natural clouds. *Journal of the Atmospheric Sciences*, *67*(10), 3303–3318. https://doi.org/10.1175/2010JAS3507.1

Hoose, C., Kristjánsson, J. E., & Burrows, S. M. (2010). How important is biological ice nucleation in clouds on a global scale? *Environmental Research Letters*, *5*(2), 024009. https://doi.org/10.1088/1748-9326/5/2/024009

Hoose, C., & Möhler, O. (2012). Heterogeneous ice nucleation on atmospheric aerosols: A review of results from laboratory experiments. *Atmospheric Chemistry and Physics*, *12*(20), 9817–9854. https://doi.org/10.5194/acp-12-9817-2012

Jensen, E. J., Diskin, G., Lawson, R. P., Lance, S., Bui, T. P., Hlavka, D., et al. (2013). Ice nucleation and dehydration in the tropical tropopause layer. *Proceedings of the National Academy of Sciences of the United States of America*, *110*, 2041–2046. https://doi.org/10.1073/pnas.1217104110

Jensen, E. J., Kärcher, B., Ueyama, R., Pfister, L., Bui, T. V., Diskin, G. S., et al. (2018). Heterogeneous ice nucleation in the tropical tropopause layer. *Journal of Geophysical Research: Atmospheres*, *123*(12), 12210–12227. https://doi.org/10.1029/2018JD028949

Jensen, E. J., Lawson, R. P., Bergman, J. W., Pfister, L., Bui, T. P., & Schmitt, C. G. (2013). Physical processes controlling ice concentrations in synoptically forced, midlatitude cirrus. *Journal of Geophysical Research*, *118*, 5348–5360. https://doi.org/10.1002/jgrd.50421

Jensen, E. J., & Pfister, L. (2004). Transport and freeze-drying in the tropical tropopause layer. *Journal of Geophysical Research*, *109*. https://doi.org/10.1029/2003JD004022

Jensen, E. J., Pfister, L., Bui, T.-P., Lawson, P., & Baumgardner, D. (2010). Ice nucleation and cloud microphysical properties in tropical tropopause layer cirrus. *Atmospheric Chemistry and Physics*, *9*, 20631–20675. https://doi.org/10.5194/acpd-9-20631-2009

Jensen, E. J., Pfister, L., Jordan, D. E., Bui, T. V., Ueyama, R., Singh, H. B., et al. (2016). The NASA Airborne Tropical TRopopause EXperiment (ATTREX): High-altitude aircraft measurements in the tropical Western Pacific. *Bulletin of the American Meteorological Society*. https://doi.org/10.1175/BAMS-D-14-00263.1

Jensen, E. J., Pfister, L., & Toon, O. B. (2011). Impact of radiative heating, wind shear, temperature variability, and microphysical processes on the structure and evolution of thin cirrus in the tropical tropopause layer. *Journal of Geophysical Research: Atmospheres*, *116*, 1–9. https://doi.org/10.1029/2010JD015417

Jensen, E. J., Thornberry, T. D., Rollins, A. W., Ueyama, R., Pfister, L., Bui, T., et al. (2017). Physical processes controlling the spatial distributions of relative humidity in the tropical tropopause layer over the Pacific. *Journal of Geophysical Research: Atmospheres*, *122*, 6094–6107. https://doi.org/10.1002/2017JD026632

Jensen, E. J., Toon, O. B., Pfister, L., & Selkirk, H. B. (1996). Dehydration of the upper troposphere and lower stratosphere by subvisible cirrus clouds near the tropical tropopause. *Geophysical Research Letters*, *23*(8), 825–828. https://doi.org/10.1029/96GL00722

Jensen, E. J., Toon, O. B., Tabazadeh, A., Sachse, G. W., Anderson, B. E., Chan, K. R., et al. (1998). Ice nucleation processes in upper tropospheric wave-clouds observed during SUCCESS. *Geophysical Research Letters*, *25*(9), 1363–1366. https://doi.org/10.1029/98GL00299

Kärcher, B., & Burkhardt, U. (2008). A cirrus cloud scheme for general circulation models. *Quarterly Journal of the Royal Meteorological Society*, *134*, 1439–1461. https://doi.org/10.1002/qj

Kay, J. E., Hillman, B. R., Klein, S. A., Zhang, Y., Medeiros, B., Pincus, R., et al. (2012). Exposing global cloud biases in the Community Atmosphere Model (CAM) using satellite observations and their corresponding instrument simulators. *Journal of Climate*, *25*, 5190–5207. https://doi.org/10.1175/JCLI-D-11-00469.1

Keese, R. G. (1989). Nucleation and particle formation in the upper atmosphere. *Journal of Geophysical Research*, *94*(14), 683–692. https://doi.org/10.1029/JD094iD12p14683

Koop, T., Luo, B., Tsias, A., & Peter, T. (2000). Water activity as the determinant for homogeneous ice nucleation in aqueous solutions. *Nature*, *406*, 611–614. https://doi.org/10.1038/35020537

Lamarque, J. F., Emmons, L. K., Hess, P. G., Kinnison, D. E., Tilmes, S., Vitt, F., et al. (2011). CAM-CHEM: Description and evaluation of interactive atmospheric chemistry in the community Earth System Model. *Geoscientific Model Development*, *5*, 369–411. https://doi.org/10.5194/gmd-5-369-2012

Lawson, R. P., O'Connor, D., Zmarzly, P., Weaver, K., Baker, B., Mo, Q., & Jonsson, H. (2006). The 2D-S (STEREO) probe: Design and preliminary tests of a new airborne, high-speed, high-resolution particle imaging probe. *Journal of Atmospheric and Oceanic Technology*, *23*, 1462–1477. https://doi.org/10.1175/JTECH1927.1

Lin, J. L. (2007). The double-ITCZ problem in IPCC AR4 coupled GCMs: Ocean-atmosphere feedback analysis. *Journal of Climate*, *20*(18), 4497–4525. https://doi.org/10.1175/JCLI4272.1

Liu, X., Easter, R. C., Ghan, S. J., Zaveri, R., Rasch, P., Shi, X., et al. (2012). Toward a minimal representation of aerosols in climate models: Description and evaluation in the Community Atmosphere Model CAM5. *Geoscientific Model Development*, *5*(3), 709–739. https://doi.org/10.5194/gmd-5-709-2012

Liu, X., Shi, X., Zhang, K., Jensen, E. J., Gettelman, A., Barahona, D., et al. (2012). Sensitivity studies of dust ice nuclei effect on cirrus clouds with the Community Atmosphere Model CAM5. *Atmospheric Chemistry and Physics*, *12*, 12061–12079. https://doi.org/10.5194/acp-12-12061-2012

Loeb, N. G., Doelling, D. R., Wang, H., Su, W., Nguyen, C., Corbett, J. G., et al. (2018). *Clouds and the Earth's Radiant Energy System (CERES) Energy Balanced and Filled (EBAF) Top-of-Atmosphere (TOA) Edition-4.0 data product* (Vol. 31, pp. 895–918). American Meteorological Society. https://doi.org/10.1175/JCLI-D-17-0208.1

Lohmann, U. (2002). A glaciation indirect aerosol effect caused by soot aerosols. *Geophysical Research Letters*, *29*(4), 8–11. https://doi.org/10.1029/2001gl014357

Maloney, C., Bardeen, C., Toon, O. B., Jensen, E., Woods, S., Thornberry, T., et al. (2019). An evaluation of the representation of tropical tropopause cirrus in the CESM/CARMA model using satellite and aircraft observations. *Journal of Geophysical Research: Atmospheres*, *124*, 8659–8687. https://doi.org/10.1029/2018JD029720

Mechoso, C. R., Robertson, A. W., Barth, N., Davey, M. K., Delecluse, P., Gent, P. R., et al. (1995). The seasonal cycle over the tropical Pacific in coupled ocean-atmosphere general circulation models. *Monthly Weather Review*, *123*(9), 2825–2838. https://doi.org/10.1175/1520-0493(1995)123<2825:tscott>2.0.co;2

Meyers, M. P., DeMott, P. J., & Cotton, W. R. (1992). New primary ice-nucleation parameterizations in an explicit cloud model. *Journal of Applied Meteorology and Climatology*, *31*(7), 708–721. https://doi.org/10.1175/1520-0450(1992)031<0708:NPINPI>2.0.CO;2

Morrison, H., & Gettelman, A. (2008). A new two-moment bulk stratiform cloud microphysics scheme in the community atmosphere model, version 3 (CAM3). Part I: Description and numerical tests. *Journal of Climate*, *21*, 3642–3659. https://doi.org/10.1175/2008JCLI2105.1

Murphy, D. M., Cziczo, D. J., Froyd, K. D., Hudson, P. K., Matthew, B. M., Middlebrook, A. M., et al. (2006). Single-particle mass spectrometry of tropospheric aerosol particles. *Journal of Geophysical Research*, *111*, 1–15. https://doi.org/10.1029/2006JD007340

Neelin, J. D., & Dijkstra, H. A. (1995). Ocean-atmosphere interaction and the tropical climatology. Part I: The dangers of flux correction. *Journal of Climate*, *8*(5), 1325–1342. https://doi.org/10.1175/1520-0442(1995)008<1325:OAIATT>2.0.CO;2

Pruppacher, H. R., & Klett, J. D. (1997). *Microphysics of clouds and precipitation* (2nd ed.). Kluwer Academic Publishers. Retrieved from https://books.google.com/books?id=Nk40jwEACAAJ

Randel, W. J., & Jensen, E. J. (2013). Physical processes in the tropical tropopause layer and their roles in a changing climate. *Nature Geoscience*, *6*(3), 169–176. https://doi.org/10.1038/ngeo1733

Rapp, M., & Thomas, G. E. (2006). Modeling the microphysics of mesospheric ice particles: Assessment of current capabilities and basic sensitivities. *Journal of Atmospheric and Solar-Terrestrial Physics*, *68*, 715–744. https://doi.org/10.1016/j.jastp.2005.10.015

Rasch, P. J., & Kristjánsson, J. E. (1998). A comparison of the CCM3 model climate using diagnosed and predicted condensate parameterizations. *Journal of Climate*, 1587–1614.

Ringer, M. A., Mcavaney, B. J., Andronova, N., Buja, L. E., Esch, M., Ingram, W. J., et al. (2006). Global mean cloud feedbacks in idealized climate change experiments. *Geophysical Research Letters*, *33*. https://doi.org/10.1029/2005GL025370

Rosenfield, J. E., Considine, D. B., Schoeberl, M. R., & Browell, E. V. (1998). The impact of subvisible cirrus clouds near the tropical tropopause on stratospheric water vapor. *Geophysical Research Letters*, *25*(11), 1883. https://doi.org/10.1029/98GL01294

Rossow, W. B., & Schiffer, R. A. (1999). Advances in understanding clouds from ISCCP. *Bulletin of the American Meteorological Society*, *80*(11), 2261–2287. https://doi.org/10.1175/1520-0477(1999)080<2261:AIUCFI>2.0.CO;2

Stephens, G. L., Vane, D. G., Tanelli, S., Im, E., Durden, S., Rokey, M., et al. (2008). CloudSat mission: Performance and early science after the first year of operation. *Journal of Geophysical Research*, *113*, 1–18. https://doi.org/10.1029/2008JD009982

Thomson, D. S., Schein, M. E., Murphy, D. M., Thomson, D. S., Schein, M. E., & Particle, D. M. M. (2000). *Particle analysis by laser mass spectrometry WB-57F instrument overview* (p. 6826). https://doi.org/10.1080/027868200410903

Toon, O. B., Maring, H., Ferrare, R., Jacob, D. J., Jensen, E. J., Luo, Z. J., et al. (2016). Planning, implementation, and scientific goals of Studies of Emissions and Atmospheric Composition, Clouds, and Climate Coupling by Regional Surveys (SEAC^{4}S) field mission. *Journal of Geophysical Research: Atmospheres*, *121*, 4967–5009. https://doi.org/10.1002/2015JD024297.Received

Toon, O. B., Starr, D. O., Jensen, E. J., Newman, P. A., Platnick, S., Schoeberl, M. R., et al. (2010). Planning, implementation, and first results of the Tropical Composition, Cloud and Climate Coupling Experiment (TC^4). *Journal of Geophysical Research*, *115*, 1–33. https://doi.org/10.1029/2009JD013073

Toon, O. B., Turco, R. P., Westphal, D., Malone, R., & Liu, M. S. (1988). A multidimensional model for aerosols: Description of computational analogs. *American Meteorological Society*, *45*(15), 2123–2144. https://doi.org/10.1175/1520-0469(1988)045<2123:AMMFAD>2.0.CO;2

Trainer, M. G., Toon, O. B., & Tolbert, M. A. (2009). Measurements of depositional ice nucleation on insoluble substrates at low temperatures: Implications for Earth and Mars. *Journal of Physical Chemistry C*, *113*(6), 2036–2040.

Turco, R. P., Hamill, P., Toon, O. B., Whitten, R. C., & Kiang, C. S. (1979). A one-dimensional model describing aerosol formation and evolution in the stratosphere: I. Physical processes and mathematical analogs. *American Meteorological Society*, *36*, 699–717.

Vaughan, M. A., Winker, D. M., & Powell, K. A. (2005). *CALIOP algorithm theoretical basis document. Part 2: Feature detection and layer properties algorithms* (pp. 1–87).

Waliser, D. E., Li, J. F., Woods, C. P., Austin, R. T., Bacmeister, J., Chern, J., et al. (2009). Cloud ice: A climate model challenge with signs and expectations of progress. *Journal of Geophysical Research*, *114*. https://doi.org/10.1029/2008JD010015

Wang, H., Easter, R. C., Rasch, P. J., Wang, M., Liu, X., Ghan, J., et al. (2013). Sensitivity of remote aerosol distributions to representation of cloud-aerosol interactions in a global climate model. *Geoscientific Model Development*, 765–782. https://doi.org/10.5194/gmd-6-765-2013

Wang, P.-H., McCormick, M. P., Poole, L. R., Chu, W. P., Yue, G. K., Kent, G. S., & Skeens, K. M. (1994). Tropical high cloud characteristics derived from SAGE II extinction measurements. *Atmospheric Research*, *34*(1–4), 53–83. https://doi.org/10.1016/0169-8095(94)90081-7

Wang, Y., Liu, X., Hoose, C., & Wang, B. (2014). Different contact angle distributions for heterogeneous ice nucleation in the Community Atmospheric Model version 5. *Atmospheric Chemistry and Physics*, *14*, 10411–10430. https://doi.org/10.5194/acp-14-10411-2014

Waters, J. W., Froidevaux, L., Harwood, R. S., Jarnot, R. F., Pickett, H. M., Read, W. G., et al. (2006). The Earth Observing System Microwave Limb Sounder (EOS MLS) on the Aura Satellite. *IEEE Transactions on Geoscience and Remote Sensing*, *44*(5), 1075–1092.

Wheeler, M. J., & Bertram, A. K. (2012). Deposition nucleation on mineral dust particles: A case against classical nucleation theory with the assumption of a single contact angle. *Atmospheric Chemistry and Physics*, *12*(2), 1189–1201. https://doi.org/10.5194/acp-12-1189-2012

Wilson, D., & Ballard, S. (1999). A microphysically based precipitation scheme for the UK Meteorological Office Unified Model. *Quarterly Journal of the Royal Meteorological Society*, *125*, 1607–1636. https://doi.org/10.1002/qj.49712555707

Winker, D. M., Hostetler, C., Vaughan, M., & Omar, A. (2006). *CALIOP algorithm theoretical basis document. Part 1: CALIOP instrument and algorithm overview* (pp. 1–29).

Winker, D. M., Hunt, W. H., & McGill, M. J. (2007). Initial performance assessment of CALIOP. *Geophysical Research Letters*, *34*. https://doi.org/10.1029/2007GL030135

Winker, D. M., Pelon, J., Coakley, J. A., Jr., Ackerman, S. A., Charlson, R. J., Colarco, P. R., et al. (2010). The CALIPSO mission: A global 3D view of aerosols and clouds. *Bulletin of the American Meteorological Society*. https://doi.org/10.1175/2010BAMS3009.1

Winker, D. M., Pelon, J., & Mccormick, M. P. (2003). The CALIPSO mission: Space-borne lidar for observation of aerosols and clouds. In U. N. Singh, T. Itabe, & Z. Liu (Eds.), *Lidar Remote Sensing for Industry and Environment Monitoring III* (pp. 1–11, Vol. 4893). International Society for Optical Engineering (SPIE Proceedings).

Winker, D. M., Vaughan, M. A., Omar, A., Hu, Y., Powell, K. A., Liu, Z., et al. (2009). Overview of the CALIPSO mission and CALIOP data processing algorithms. *Journal of Atmospheric and Oceanic Technology*, *26*, 2310–2323. https://doi.org/10.1175/2009JTECHA1281.1

Yang, Q., Easter, R. C., Campuzano-jost, P., Jimenez, J. L., Fast, J. D., Ghan, S. J., et al. (2015). Aerosol transport and wet scavenging in deep convective clouds: A case study and model evaluation using a multiple passive tracer analysis approach. *Journal of Geophysical Research: Atmospheres*, 8448–8468. https://doi.org/10.1002/2015JD023647.Received

Yang, Q., Fu, Q., & Hu, Y. (2010). Radiative impacts of clouds in the tropical tropopause layer. *Journal of Geophysical Research*, *115*. https://doi.org/10.1029/2009JD012393

Young, K. C. (1974). The role of contact nucleation in ice phase initiation in clouds. *Journal of the Atmospheric Sciences*, *31*(3), 768–776. https://doi.org/10.1175/1520-0469(1974)031<0768:TROCNI>2.0.CO;2

Yu, P., Froyd, K. D., Portmann, R. W., Toon, O. B., Freitas, S. R., Bardeen, C. G., et al. (2019). Efficient in-cloud removal of aerosols by deep convection geophysical research letters. *Geophysical Research Letters*, *46*, 1–9. https://doi.org/10.1029/2018GL080544

Zhang, M. H., Lin, W. Y., Klein, S. A., Bacmeister, J. T., Bony, S., Cederwall, R. T., et al. (2005). Comparing clouds and their seasonal variations in 10 atmospheric general circulation models with satellite measurements. *Journal of Geophysical Research*, *110*. https://doi.org/10.1029/2004JD005021